PRODUCTION OF ALUMINA BASED POROUS CERAMICS USING SODIUM ALGINATE AS GELLING AGENT

A Thesis Submitted

In Partial Fulfillment of the Requirement

For the degree of

BACHELOR OF TECHNOLOGY

By

ABINASH PRADHAN

ROLL 110CR0611

TO THE

DEPARTMENT OF CERAMIC ENGINEERING

NATIONAL INSTITUTE OF TECHNOLOGY ROURKELA

MAY 2014

CERTIFICATE

This is certified that the work contained in the project entitled "PRODUCTION OF ALUMINA BASED POROUS CERAMICS USING SODIUM ALGINATE AS GELLING AGENT" by Abinash Pradhan (Roll 110CR0611) in partial fulfillment of the requirements of the award of Bachelor of Technology Degree in Ceramic Engineering at National Institute of Technology, Rourkela is an authentic work carried out by him under my supervision and guidance.

To the best of my knowledge, the matter embodied in the thesis has not been submitted to any other university / institute for the award of any Degree or Diploma.

ARUN CHOWDHURY
ASSISTANT PROFESSOR
Department of Ceramic Engineering
National Institute of Technology
Rourkela-769008

ACKNOWLEDGEMENT

I express my deep gratitude to my guide, Prof. Arun Chowdhury, Department of Ceramic Engineering, NIT Rourkela, for his valuable advice, time and guidance in the completion of this project work. My heartfelt thanks to all the faculty members for their suggestions during this project work.

My sincere acknowledgement to the Research Scholars, M. Tech students and the non-teaching staff for their help and cooperation extended to me.

And finally, my heartful thanks to all my friends who have constantly helped, encouraged, boosted my morale and have worked with me in completing this dissertation work.

Abinash Pradhan

110CR0611

LIST OF FIGURES:

LIST OF TABLES:

CONTENTS

ABSTRACT

Porous ceramics are increasingly becoming important in catalytic support and filtration, especially in waste management and recovery of materials. In this report, we reviewd the main processing routes that can be used for the fabrication of macroporous ceramics with tailored microstructure. Emphasis is given to versatile and simple approaches that allow one to control the microstructural features that ultimately determine the properties of the macroporous material. In the present study effort had been given to understand the interrelation of microstructure and specific surface area of millimetric beads of gamma-alumina. Aluminium Oxihydroxide (boehmite) was used to exploit fast gelation with sodium alginate by ion exchange. This gelation mechanism led to the preparation of bodies that can be more easily manipulated than powders. The project work focuses on the production of alumina based porous ceramics and its characterization with 3 different alumina samples having solid loading of boehmite (12-36) percent were prepared by sol-gel process. Alumina beads were calcined in the temperature range ($900^{O}C–1100^{O}C$) for 2 hours. The beads were then characterized by X-ray Diffraction, Scanning Electron Microscopy, BET surface area and mechanical strength measurement. The microstructure reveals the distribution of the pores inside those beads and the average size of pores. The specific surface area of the beads with 24% and 36 % solid loading at 900°C is found to be 119.50 m^2/g and 126.06 m^2/g respectively. The present work discusses the most important aspects to take into consideration of the improvement of γ- Al_2O_3 as a support for catalytic applications. We show that the synthetic route to γ-Al_2O_3 is the starting point that determines the micro- and macrostructure of the oxide and, consequently, important physical and mechanical properties.

CHAPTER-1:

INTRODUCTION

1.1. ***Introduction:***

Pores and pore size distribution in materials can affect performance, properties, strength (both flexural and compressive), and density of materials. In applications of porous material, transport through the pore phase is very important which can be achieved if the materials contain more than 50% connected porosity. Porous ceramics have received considerable interest in studies and have been used as hot gas or molten metal filters, catalyst carriers, and separation membranes, because of their excellent mechanical properties, high-temperature resistance, and chemical stability. [1]

Processes like polymer foam impregnation, gel casting, freeze drying and tape casting have been used for the consolidation of the powder suspensions into porous bodies. Gel casting produces porous ceramics with a combination of open and closed pore microstructure having superior mechanical properties in wide range of porosities. Porous ceramics have become more important recently, because they are used as filters in particulate gas filtration to reduce environmental pollution in various industrial fields. For example, cordierite ceramic honeycomb substrates coated with catalysts have been widely used as diesel particulate filters, to control automotive exhaust emissions. [2]

Fig. 1.1. Picture of Porous Ceramics

Pore size control is the key factor in fabrication of porous materials. Also particle size distribution of the raw materials, processing techniques and sintering affect the final porosity and pore connectivity. [3]

Alumina is used for making porous ceramics because most of the alumina-based ceramics possess relatively high strength along with improved thermal stability. Because of their inherently brittle nature, pores have been traditionally avoided in ceramic components because pores reduce the material's strength. However, applications of porous ceramics have increased in the last decades, especially for environments where high temperatures, excessive wear and corrosive environment are involved.[4] Such applications include the filtration of molten metals, high-temperature thermal insulation, support for catalytic reactions, and filtration of hot corrosive gases in various industrial operations.[5]

Porous ceramics are used good at aforementioned applications due to the following advantages like high melting point, high corrosion resistance and wear resistance along with the features gained by the replacement of solid material by voids in the material. Such features include low thermal mass, low thermal conductivity, controlled permeability, high surface area, low density and high specific strength. These properties can be modified for each specific application by controlling the composition and microstructure of the porous ceramic. Fluctuations in open and closed porosity, pore size distribution, and pore morphology can have a major effect on a material's properties. These microstructural features are in turn are greatly influenced by the processing route used for the production of the porous material. Porous ceramics are generally prepared by the polymer-sponge method, foaming method or by the gel casting method. [6]

The synthesis of support material has been receiving recently great attention with increasing concern about the heterogeneous catalyst. Among the different transition aluminas known, γ-Al_2O_3 is perhaps the most important with direct application as a catalyst or catalytic support in the automotive and petroleum industries. In catalysis, γ-alumina is preferred because it can provide high surface area and thermal stability which are suitable characteristics for catalytic performance.

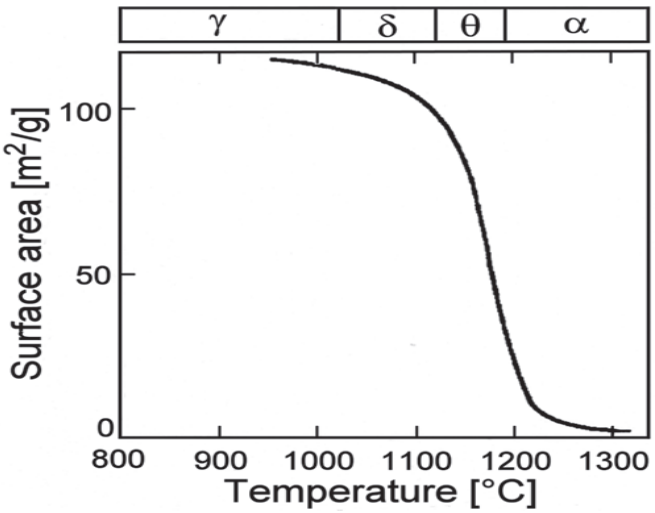

Figure 1.2. Phase transformations and specific surface area of Alumina

The importance of alumina as catalyst or catalytic support has also been widely recognized for many chemical reactions [7]. It is believed that the properties of such alumina particles are largely governed by the particle size, morphology, surface and phase homogeneity which can be controlled by selecting a proper synthetic route [8]. γ-Alumina with desirable surface properties such as high surface area and mesoporous properties is most commonly used as a high-temperature catalyst or catalytic support. The synthesis of alumina by sol-gel technique generally produces a mixture of alumina phases (Θ, γ and δ) and these transform to a stable α-alumina phase by heating at comparatively high temperature (1200°C). [9]

In the present work a new concept is illustrated describing how one can take advantage of two different gelation mechanisms, one involving fast gelation of a biopolymer, sodium alginate and the other based on gelation of mineral species boehmite, a well known aluminium oxihydroxide.

Sodium alginate used is a natural biopolymer extracted from algae that is used as a gelling additive. One of its main properties is its capability to gel when the sodium ion is substituted by a multivalent cation (usually Ca(II)) that builds cross-section between the polymer chains. This property was used for the preparation of organic millimetric beads that could retain

active molecules further used for drug release, metal biosorption, filtration membranes and many more.

The present report describes an example of combination between gelifying properties of boehmite and sodium alginate to obtain millimetric beads with high surface area and narrow pore size distribution.

1.2. **Need of Porous ceramics as catalyst**

Porous ceramics are increasingly becoming important in particulate gas filtration. These classes of ceramics are essential for many industries where high permeability, high surface area, and insulating characteristics are required. The search for porous ceramics with good mechanical strength has stimulated the development of several technologies.

Porous ceramics fabricated by gelcasting bring many unique capabilities in mitigating environmental issues, particularly waste recycling and neutralization of hazardous emissions. Potential opportunities for using gelcasting technique in setting mechanically foamed slurry can be described by adaptable designing and modification of the foamed slurry characteristics with a goal of preserving the environment.

One of the attractive ways of tailoring the material well-suited to environmental concern is the incorporation of pores within a ceramic microstructure that gives many unique properties such as high permeability, high surface area, good insulating characteristics, etc. These properties make porous ceramics suitable for a wide range of applications such as filters, membranes, sensors, catalyst carriers, piezoelectric ceramics, biomedical and construction materials. Recently, applications for separation filters have become important to reduce environmental pollution in various fields.

CHAPTER-2: LITERATURE REVIEW

Porous ceramics are nowadays being investigated for a variety of applications including molten metal and hot gas filters, light- weight structural components, electrodes, sensors, bioreactors, catalyst carriers, radiant burners and as porous implant in the area of biomaterials due to their specific properties like high surface area, high temperature stability, high permeability, low weight and low thermal conductivity.

2.1 **Types of Porous Ceramics**

Porous ceramic products can be categorized according to the following specifications: [10]

- Chemical composition of raw material: alumino-silicate, silicate, oxide, non-oxide etc.
- Porosity: moderate (30-50%), high porosity (60-75%), and super-high porosity (over 75%)
- Inner structure: granular, cellular, fibrous
- Refractoriness correlated to service temperatures: low-melting (below 1350°C), high melting (1350-1580°C), refractory (1580-1770°C), highly refractory (1770-2000°C),
- Destination and application area: heat insulating (main parameter: thermal conductivity); heat shielding (main parameter: product of heat conductivity and apparent density values), and permeable (main parameters: porosity, pore size and permeability)

Porous ceramics are generally divided into two categories: reticulate ceramics and foam ceramics. A reticulate ceramic consists of interconnected voids surrounded by a web of ceramic struts and is fabricated by infiltration and replication of a polymeric sponge perform. Ceramic foam consists of closed and open pores within a continuous ceramic matrix and is usually made by foaming processes applying foaming agents or by powder consolidation using fugitive organic additives as pore formers. [11]

The two types of porous ceramics mentioned above exhibit nearly isotropic pore morphology but differ in the porosity, size and shape of pores and permeability. Permeability is high in reticulate ceramics as compared to open or closed pore foam ceramics due to the larger pore size as well as open pore structure.

O. Lyckfeldt et al. [12] developed a new method for forming porous ceramics by using starch as both binder and pore former. Simple and complex shaped components of porous alumina were shaped and demoulded in wet state in this method. After drying, burnout and sintering, materials with porosities between 23 and 70% were obtained.

2.2 **Fabrication of Porous Ceramics**

The development of porous ceramic materials has provided a new challenge to several industries, because porous ceramics are more durable in extreme environments and their surface characteristics permit them to fulfill very specific requirements. Presently, different porous ceramics with more delicate and uniform pore structures, having wide pore size range (few micrometers to a few nanometers) can be prepared for diverse purposes via varied physical and chemical processing.

R. Svinka et al. [13] studied the production of porous alumina ceramics by slurry casting method and investigated pore formation by elimination of hydrogen as a result of a chemical reaction of aluminum powder with water. The purpose of the study was to determine various ways of producing high porosity alumina ceramics having high mechanical strength and other high temperature properties of porous ceramics.

Kajutaka Kamitani et al. [14] fabricated highly porous alumina based ceramics by slip casting method employing polymethylmethacrylate (PMMA) microspheres having different diameters as a template and MgO/SiC powder as a sintering aid and subsequent calcinations at 1600°C. The sintered product contained spherical pores relating to the morphology of PMMA microspheres. Highly porous and mechanically strong alumina ceramics having an open porosity of 62%, a connected space size of 1.3μm, and a compressive strength of 147.6 MPa was fabricated.

Various processing have been developed which have used replica, sacrificial template or direct foaming methods for the production of various porous ceramics.

2.2.1. **Replica Technique**

The replica method involves the impregnation of a cellular structure with a ceramic suspension for the production of a porous ceramic showing the same morphology as the original porous material. Many natural and synthetic cellular structures are used as templates to fabricate porous ceramics through this technique.

(1) ***Synthetic templates***

Sponge replica technique is one of the best processing methods for porous ceramics and is used in industry to prepare ceramic filters for molten metal filtration and other useful applications. The polymer replica technique is a well-established method to prepare open cellular structures with pore sizes ranging from 200 mm to 3 mm at between 40% and 95% porosity. [15]

In the polymer replica approach, a highly porous polymeric sponge (typically polyurethane) is initially soaked into a ceramic suspension until the internal pores are filled in with ceramic material. The impregnated sponge is then passed through rollers to remove the excess suspension and enabled the formation of a thin ceramic coating over the struts of the original cellular structure.

The rheology of the impregnating suspension and its adhesion on the polymeric sponge are the most essential steps in this method. Due to high interconnectivity between pores, the permeability of fluids and gases is enhanced through the porous structure making these reticulated materials desirable for high through-put filtration. [16] Despite the easiness of this technique, the mechanical strength of cellular structures processed through this route can be considerably degraded by the formation of cracked struts during pyrolysis of the polymeric sponge. [17]

Sherman et al. [18] developed a similar process to the original replica method, where the polymeric sponge is first converted into a vitreous carbon skeleton and is subsequently infiltrated with reactive gaseous species to form macroporous ceramics of many different carbides, oxides, borides, nitrides, and silicides.

Miqin Zhang et al. [19] introduced a new technique by combining the gel-casting and polymer sponge methods to prepare macroporous hydroxyapatite scaffolds, which provides a more effective control over the microstructures of scaffolds and helps in enhancing their mechanical properties. The scaffolds thusprepared have an open, uniform and interconnected porous structure with a pore size of 200–400 mm. Compressive yield strength of ~5 MPa and a compressive modulus of ~8 GPa was attained.

(2) ***Natural templates***

Natural replica templates include the cellular structures available in nature, which are used for fabrication of porous ceramics, mainly due to their special pore morphology and intricate microstructures. In recent years, a novel replica approach has been developed that uses wood structures as positive templates.

Porous ceramics having highly oriented open pores ranging from 10 to 300 mm can be developed with this method at porosity levels between 25% and 95%. [20] The most crucial processing step in this route is the conversion of the wood-derived carbon preform into a ceramic phase. The availability of templates exhibiting the desired microstructure is also essential in this process.

J. Cao et al. [21] found a new method for preparation of microcellular ceramic materials through reproduction of wood morphologies by biotemplating. Biomorphic Al_2O_3-ceramics were produced by repeated infiltration of low viscous alumina sols into wood perform via the sol-gel route and then, sintered in air at $1550^{O}C$. X-ray diffraction (XRD), scanning electron microscopy (SEM), density and porosimetry measurements were done in order to know about the microstructure and phase formation during processing. Depending on the initial wood template, the microstructure of the highly porous alumina ceramics is characterized by uniaxial pore morphology with pore diameter in the micrometer range.

The anisotropic nature of cellular ceramics produced using wood as template might be very advantageous in applications that require open and highly oriented porous structures, such as in catalysis and in the filtration of liquids and hot gases.[22] As a result of their highly oriented structures, the mechanical properties of wood-derived ceramics are markedly

anisotropic. The mechanical strength in the axial direction (along the oriented pores) is considerably higher than that in the tangential/perpendicular direction. Structures with high mechanical strength can only be achieved when the carbon preform is totally converted into the ceramic phase. [23]

2.2.2. **Sacrificial Template Method**

The sacrificial template technique includes preparation of a biphasic composite consisting of a continuous matrix of ceramic particles or ceramic precursors and a dispersed sacrificial phase that is initially homogeneously distributed throughout the matrix and is finally extracted to generate pores within the microstructure. Sacrificial templating methods provide an alternative for the fabrication of porous ceramics with porosities and average pore sizes ranging from 20% to 90% and 1–700 mm, respectively.[14]

The most important step in this technique is the removal of the sacrificial phase by pyrolysis, evaporation, or sublimation. This process might involve the release of an excessive amount of gases and have to be carried out at sufficiently slow rates in order to avoid cracking of the cellular structure. The mechanical strength of cellular structures formed by this method is considerably higher than that achieved with the replica techniques.

Macroporous ceramics obtained with the template method display compressive strengths typically within the range predicted for open and closed-cell structures. Fig. 2.1 exhibits the images of microstructures of macroporous ceramics produced with the sacrificial template method.

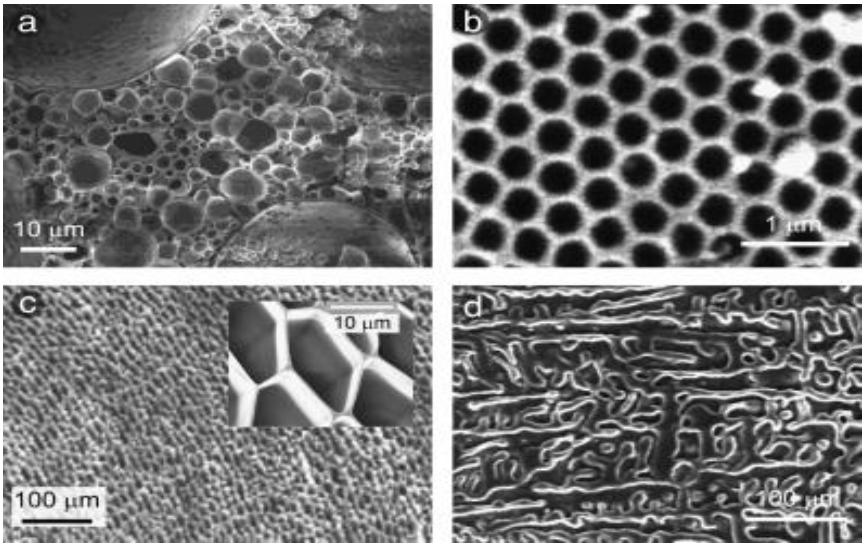

Fig 2.1. Microstructures of macroporous ceramics produced with the sacrificial template method. (a) TiO_2 foam exhibiting hierarchical porous structure produced via emulsion templating (b) ordered macroporous SiO_2 obtained using polystyrene beads as templates (c) highly oriented SiO_2 honeycomb structure achieved via the unidirectional freeze-drying of silica gels (d) macroporous Al_2O_3 exhibiting dendrimer-like pores obtained using camphene as sacrificial template.

Synthetic and natural organics are often extracted through pyrolysis by applying long thermal treatments at temperatures between 200°C and 600°C. The long periods required for complete pyrolysis of the organic component and the extensive amount of gaseous by-products generated during this process are the main disadvantages of using organic materials as sacrificial phase.

The use of relatively volatile oils as a sacrificial phase in aqueous [24] or non-aqueous [25] emulsions is an interesting alternative for the fabrication of porous ceramics by this template method. The main advantages of this approach are:- (a) The fact that the template is easily incorporated into the continuous phase by simple agitation or mixing, (b) the very small droplet/pore sizes that can be achieved when using immiscible liquids exhibiting low interfacial energy, and (c) the mild conditions required for removal of the template.

Dibyendu Chakravarty et al. [26] fabricated high strength porous alumina by spark plasma sintering at temperatures between 1000°C and 1200°C with nanocrystalline $Al(OH)_3$ as the starting powder without any seeds, dopants or inclusions. Decomposition of the $Al(OH)_3$ produced a series of transitional alumina phases depending on sintering temperature and pressure and finally the stable alumina phase was obtained. A network of continuous pores with unimodal pore size distribution was found out by mercury porosimetry and BET surface area measurements, with the porosity ranging between 20% and 60% based on sintering conditions.

2.2.3. **Direct Foaming Methods**

In direct foaming methods, porous materials are produced by incorporating air into a suspension or liquid media, which is subsequently set in order to keep the structure of air bubble created. Direct foaming methods offer an easy, cheap, and fast way to prepare macroporous ceramics with open or closed porosities from 40% to 97%. Foams stabilized with surfactants lead to porous ceramics exhibiting average pore sizes from 35 mm to 1.2 mm. [27]

The consolidated foams are sintered at high temperatures later to obtain high-strength porous ceramics. The total porosity of directly foamed ceramics is proportional to the amount of gas incorporated into the suspension or liquid medium during the foaming method. The use of surface modified particles to stabilize the wet foam decreased the lower limit of pore sizes achievable via direct foaming to an average value as low as 10 mm. Cellular structures prepared by direct foaming usually exhibit mechanical strengths considerably higher than that of replica techniques due mainly to the absence of flaws in the cell struts. Compressive strengths as high as 16 MPa at a porosity level of 87 % to 90 % have been achieved with porous ceramics produced from particle-stabilized wet foams. [28]

Wood et al. [29] patented a process where ceramic particles are not used to impregnate already formed polymer foams, but are instead incorporated into organic solutions containing precursors of polyurethane foam. The obtained ceramic/organic mixtures are foamed by in situ gas incorporation in the presence of surfactants and finally consolidated by the thermosetting condensation reaction between polyols and polyisocyanates (polyurethane precursors). The in situ incorporation of gas occurred through the nucleation and growth of

gas bubbles upon heating (physical blowing) or chemical reaction (chemical blowing). By this method, the ceramic particles are distributed within the polymeric phase, avoiding the formation of hollow struts that usually degrade the foam final mechanical strength after pyrolysis.

Toshihiro Isobe et al. [30] prepared porous alumina ceramics having unidirectionally aligned cylindrical pores by extrusion method and compared them with porous ceramics having randomly distributed pores prepared by conventional method, and also investigated their gas permeability and mechanical properties. SEM micrographs of the porous alumina ceramics prepared, using nylon fibers as the pore former, through extrusion method showed excellent orientation of cylindrical pores. The bending strength and Weibull modulus of the extruded porous alumina ceramics with 39% porosity were 156 MPa and 17, respectively. These mechanical properties of extruded samples were estimated to be higher than those of the conventional porous alumina ceramics. The gas permeability of the extrusion samples is also found to be higher than that of the conventional samples and increases along with increase in porosity and pore size.

2.3 **Need of porous Alumina as catalytic convertor**

Automobile exhaust pollution contributes significantly to the air pollution. With fast increasing vehicle population even in developing countries, enormous amount of obnoxious emissions like CO, HC, NOx and particulate matter are being emitted. These pollutants have hazardous effects on environment and human health. Looking towards the exponential growth of vehicular population, control strategies for auto-exhaust pollution are essential. Out of various technologies available for automobile exhaust emission control, a catalytic converter is found to be the best option to control the CO, HC, and NOx emissions from petrol driven vehicles, while diesel particulate filter and oxidation catalytic converter or diesel oxidation catalyst have so far been the most potential options to control particulate emissions from diesel driven vehicles [31].

The basic function of the catalyst in a catalytic converter is to perform the following reactions in the automobile exhaust:

Oxidation of CO and HC to CO_2 and H_2O

$C_yH_n + (y+n/4)O_2 \longrightarrow yCO_2 + (n/2)H_2O$

$CO + (1/2)O_2 \longrightarrow CO_2$

$CO + H_2O \longrightarrow CO_2 + H_2$

Reduction of NO/NO_2 to N_2

$NO\ (or\ NO_2) + CO \longrightarrow 1/2N_2 + CO_2$

$NO\ (or\ NO_2) + H_2 \longrightarrow 1/2N_2 + H_2O$

$(y+n/2)NO\ (or\ NO_2) + C_yH_n \longrightarrow (y+n/4)\ N_2 + yCO_2 + (n/2)H_2O$

The catalyst is sometimes referred as the heart of catalytic converter, as it is actually responsible for treating the obnoxious gases. Although noble metal based catalysts have clearly dominated the area of auto-exhaust catalysis, mainly because of their high activity and thermal stability, their limited availability and high cost has always been a reason for the search of alternative catalysts. Their limited tailoring capability is also one aspect, which prompted for more investigations on mixed oxides, zeolites and perovskite based catalysts.

Automotive catalysts are generally available in the form of monolith ceramic as cordierite and zeolites or metal substrate. The catalyst substrates more used are composed of magnesium cordierite ($2MgO.2Al_2O_3.5SiO_2$) with a honeycomb structure, which provides a high geometric surface area, coated with γ-alumina (catalyst wash-coat). This wash-coat is designed to increase the specific surface area and promotes the catalytic reduction and oxidation of pollutants gases to more harmless ones like carbon dioxide, water and nitrogen molecular.

Catalytic control of auto-exhaust emissions is one of the most successful applications of heterogeneous catalysis, both in commercial and environmental point of views. Cordierite honeycomb monolith and corrugated metallic types of catalyst substrates are most commonly used for auto-exhaust catalytic converter. Alumina, silica, zirconia are some of the oxides

used for this purpose, most suitable and commonly used material being high specific surface area and high mechanical strength.

Alumina substrate has several advantages e.g.:-

- High thermal shock fracture resistance through an inherently low thermal expansion coefficient and high thermal stability
- Suitable porosity and pore size distribution
- Sufficient mechanical strength for their use in automotive catalytic converter
- Low cost, lighter weight, high geometric surface area and large interconnected pores.

Weijiang Xue et al. [32] successfully fabricated alumina ceramic bodies with high porosity characterized by highly ordered and unidirectional oriented pores in the micrometer range with a 5-15 wt% solid loading range, by a self- organization process of alginate sol. The obtained porous alumina ceramics had a high total porosity over 70%, most (>88%) of which were open pores, as well as have excellent permeability (K>2.16 x 10-11m²) and high compressive strength (>15MPa).

2.6. **Objective**

The preceding discussion on the processing of porous alumina reveals that processing route plays an important role for maintaining a porous structure with interconnectivity. On the basis of literature review, the following studies are being planned.

- Processing alumina based porous ceramics through biopolymer sodium alginate as the pore former.
- To study the porosity and strength as function of boehmite solid loading and calcination temperature.
- To characterize porous ceramics with respect to mechanical strength, porosity and microstructure.
- To determine the surface area through BET surface area analyzer and pore size distribution through Scanning Electron Microscope image.

CHAPTER-3: EXPERIMENTAL WORK

3.1. **Preparation of porous beads of alumina by addition of sodium alginate**

Reagents used:

1) Boehmite from Degussa, chemical formula: AlOOH
2) Sodium alginate from Merck, chemical formula: NaAlg
3) Hydrated aluminium nitrate- 6.6 g for each batch
4) HCl(conc.)- about 3 ml for each batch

3.1.1 **Sample preparation:-**

The in brief sol-gel processing flow chart for the system containing boehmite and sodium alginate is presented in Fig. 3.1.

PROCESS FLOW CHART

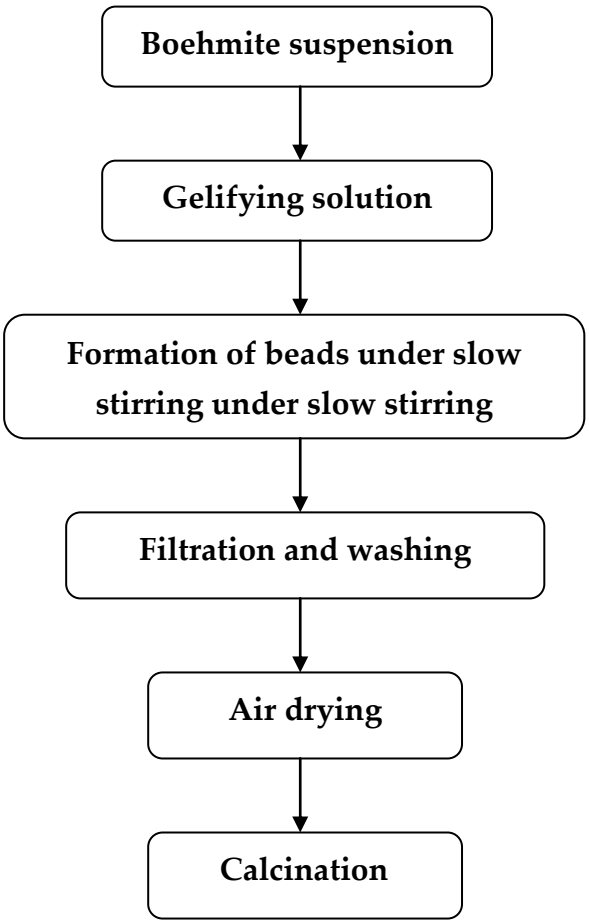

Fig. 3.1. Flow chart for preparation of calcined alumina beads

1g sodium alginate was dissolved in 50 ml of deionized water. Then different amounts of Boehmite(AlOOH) ranging from 3g to 9g was dispersed separately in 25 ml deionized water, the suspension kept under ultrasound for 2 min and stirred for 20min. After that Boehmite suspension added dropwise under magnetic stirring in the alginate solution and the suspension was kept under stirring for 20 min. The solution to complex the alginate network was prepared by dissolving 6.6 g of hydrated aluminim nitrate in 100 ml of water which was further acidified at pH<1 by addition of about 2.5 ml of conc. HCl. Then (alginate:boehmite) suspension was added dropwise into gelifying(acidic) solution under slow stirring . Drops of (alginate:boehmite) gelled and beads were formed . Beads were kept in the gelifying solution for 12 hr. The beads were recovered and neutralized by filtration and washing and then partially dehydrated by keeping in 100ml of Acetone for 12 hrs. After recovery, they were air dried for 1 day**.** After conventional drying, the beads were calcined at different temperatures i.e. 900ºC, 1000ºC and 1100ºC. At each calcination temperature, the holding time for different batch was 2 hours.

SAMPLE 1 [S112] – (3g / 25) *100% = 12% solid loading

SAMPLE 2 [S224] – (6g/25) * 100% = 24% solid loading

SAMPLE 3 [S336] – (9g/25) * 100% = 36% solid loading

3.1.2 **Photograph of dried and calcined beads**

Boehmite:6 gm
Solid loading 24%
Air dried sample

Boehmite:6 gm
Solid loading 24%
Sample calcined at 900^{O}C

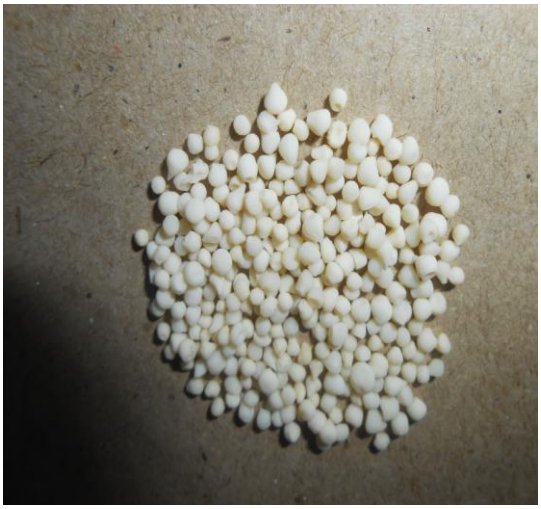

Boehmite: 9gm
Solid loading 36%
Sample calcined at 900^{O}C

Boehmite: 9gm
Solid loading 36%
Sample calcined at 900^{O}C

Fig 3.2. Photographs of dried and calcined beads

3.2 **Characterization of raw materials and calcined beads**

3.2.1 ***X-ray Diffraction (XRD)***

It is a versatile, non-destructive technique that reveals detailed information about the chemical composition and crystallographic structure of natural and manufactured materials. XRD is a powerful tool used to detect the presence of phases in the material. The main principle behind XRD is Bragg's law which states

$$n\lambda = 2d\sin\theta$$

Where, d = spacing between diffracting planes,

θ = incident angle,

n = any integer

λ = wavelength of the X-ray beam

As study of the various phases and their analysis is the main objective of this project work, XRD analysis was performed. This was done by Philips' X-ray diffractometer with Nickel filtered CuKα radiation (1.5406Å). The diffraction was done at angle 10-80^{O} with scanning

speed 2^{O}/min. Then from the XRD plot various peaks corresponding to the various phases (i.e. α, γ, Θ) were analyzed and studied.

3.2.2 *Shrinkage*

It is measured by calculating the difference between the green bead diameter and diameter of the beads after calcination at 900^{O}C. The diameter of the beads was measured by a micrometer Screw Gauge.

Linear shrinkage (%) = [(Diameter before firing – Diameter after firing)/Length before firing] ×100

Volume shrinkage (%) = [(Volume before firing – Volume after firing)/Volume before firing] ×100

3.2.3 *Scanning Electron Microscopy (SEM)*

Scanning Electron Microscope provides topographical and elemental information at magnifications of 1000X to 20,000X with unlimited depth of field. A finely focused electron beam scanned across the sample surface generates secondary electrons, backscattered electrons, and characteristic X-rays. These signals are gathered by detectors to form images of the sample displayed on a cathode ray tube screen. Data Output is generated on the CRT monitor. Images and spectra are recorded on CD ROM. Alumina beads calcined at different temperatures i.e. 900^{O}C, 1000^{O}C and 1100^{O}C for 2 hours were chosen for SEM.

3.2.4 *BET Surface area*

The specific surface area of a material is determined by physical adsorption of a gas on the surface of the solid and by calculating the amount of adsorbate gas corresponding to a monomolecular layer on the surface. Physical adsorption results from relatively weak forces (van der Waals forces) between the adsorbate gas molecules and the adsorbent surface of the test powder. The determination is usually carried out at the temperature of liquid nitrogen. The amount of gas adsorbed can be measured by a volumetric or continuous flow procedure. The data are treated according to the Brunauer, Emmett and Teller (BET) adsorption isotherm equation:

$$\frac{1}{\left[V_a\left(\frac{P_o}{P}-1\right)\right]} = \frac{C-1}{V_m C} \times \frac{P}{P_o} + \frac{1}{V_m C}$$

P = partial vapour pressure of adsorbate gas in equilibrium with the surface at 77.4 K (b.p. of liquid nitrogen), in pascals,

Po = saturated pressure of adsorbate gas, in pascals,

P/ Po = relative pressure

Va = volume of gas adsorbed at standard temperature and pressure (STP) [273.15 K and atmospheric pressure (1.013 × 105 Pa)], in millilitres,

Vm = volume of gas adsorbed at STP to produce an apparent monolayer on the sample surface, in millilitres,

C = dimensionless constant that is related to the enthalpy of adsorption of the adsorbate gas on the sample.

A value of Va is measured at each of not less than 3 values of P/Po.

Then the BET value

$$\frac{1}{\left[V_a\left(\frac{P_o}{P}-1\right)\right]}$$

is plotted against P/Po according to equation (1). This plot should yield a straight line usually in the approximate relative pressure range 0.05 to 0.3. The data are considered acceptable if the correlation coefficient, r, of the linear regression is not less than 0.9975; that is, r^2 is not less than 0.995. From the resulting linear plot, the slope, which is equal to (C −1)/*Vm*C, and the intercept, which is equal to 1/*Vm*C, are evaluated by linear regression analysis. From these values, V*m* is calculated as 1/(slope + intercept), while *C* is calculated as (slope/intercept) + 1. From the value of *Vm* so determined, the specific surface area, *S*, in $m^2 \cdot g^{-1}$, is calculated by the equation:

$$S = \frac{V_m N a}{m \times 22400}$$

N = Avogadro constant (6.023 × 1023 mol^{-1}),

a = effective cross-sectional area of one adsorbate molecule, in square metres (0.162 nm^2 for nitrogen and 0.195 nm^2 for krypton),

m = mass of adsorbate, in grams,

22400 = volume occupied by 1 mole of the adsorbate gas at STP allowing for minor departures from the ideal, in millilitres.

A minimum of 3 data points is required. Additional measurements may be carried out, especially when non-linearity is obtained at a *P*/*Po* value close to 0.3. Because non-linearity is often obtained at a *P*/*Po* value below 0.05, values in this region are not recommended. The test for linearity, the treatment of the data, and the calculation of the specific surface area of the sample are described above.

Outgassing

Before the specific surface area of the sample can be determined, it is necessary to remove gases and vapours that may have become physically adsorbed onto the surface after manufacture and during treatment, handling and storage. If outgassing is not achieved, the specific surface area may be reduced or may be variable because an intermediate area of the surface is covered with molecules of the previously adsorbed gases or vapours. The outgassing conditions are critical for obtaining the required precision and accuracy of specific surface area measurements because of the sensitivity of the surface of the materials.

3.2.5 *Cold Crushing Strength Test*

The hardness of the calcined beads was measured by Vickers Hardness Tester (Blue Star Limited, VM-50, India). The vicker hardness of the beads were calculated by using the following formula.

$$Hv = 1.854(F/D^2)$$

Where,

Hv in newton

F being the applied load measured in kgf

D is the half of the diagonal length of the indentation in mm.

CHAPTER-4:

RESULTS

AND

DISCUSSIONS

4.1 ***Shrinkage***

The linear shrinkage and volume shrinkage(assuming isotropic shrinkage) of the calcined beads (all samples calcined at 900 ^{o}C) with different solid loading are as follows:

Table 4.1 Linear and Volume shrinkage of beads calcined at 900^{O}C having different solid loading

Boehmite solid loading	***Average Linear shrinkage (%)***	***Average Volume shrinkage (%)***
12%	2.89	8.366
24%	2.343	6.238
36%	1.730	5.095

The extent of shrinkage due to calcination is different for different calcination temperature and that tends to decrease with increasing solid loading. The change in such physical property could be attributed to the fact that the shrinkage in drying is constraint as the solid loading increases. The average initial volume of the shaped beads were almost identical. So the samples with low solid loading are having much more shrinkage after calcination.

4.2 ***X-ray Diffraction (XRD)***

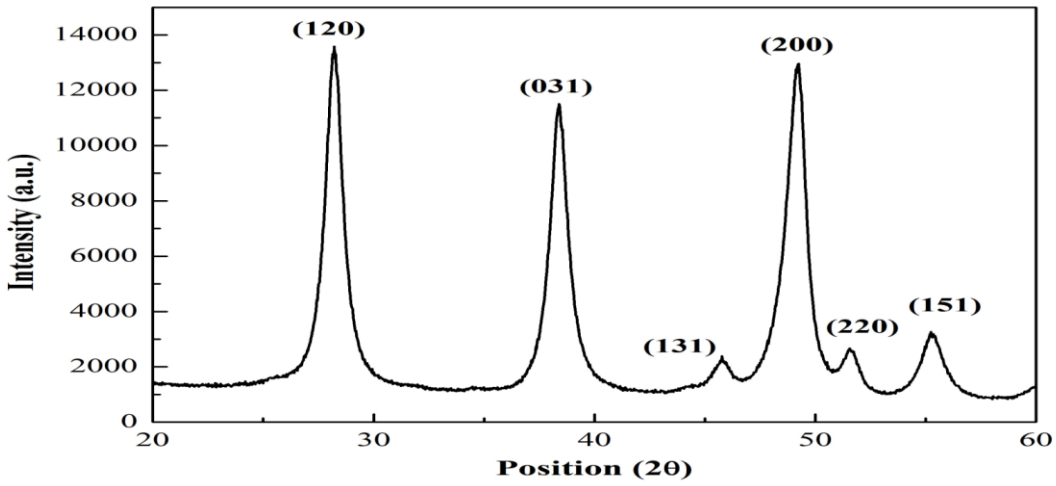

Fig. 4.1 Diffration pattern of raw boehmite (AlOOH)

The above figure shows the diffraction pattern of raw 'boehmite' which was used as the starting material. X-ray diffraction counts were taken from 2Θ value 20-60^{O}. As per standard JCPDS file no. 83-2314 another major diffraction peak is observed at plane (020) and it becomes clear that boehmite (AlOOH) belongs to orthorhombic crystal system of the space group ***Amam*** and having space group number 63.

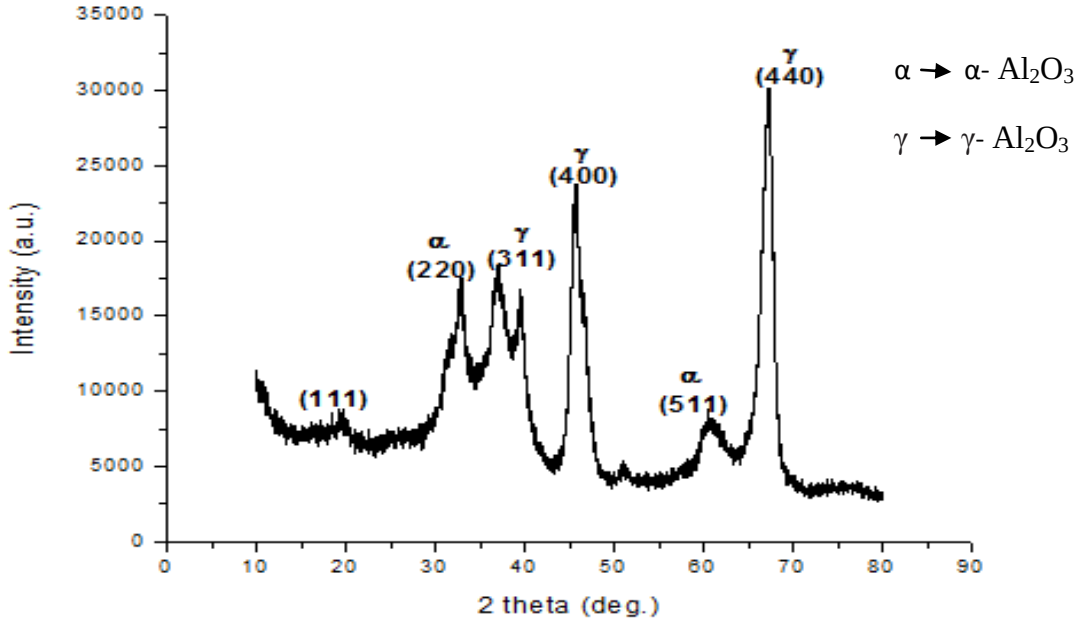

Fig. 4.2 Diffraction pattern of alumina beads (12% solid loading of boehmite) calcined at 900^{O}C

The above figure shows the diffraction pattern of porous alumina beads calcined at 900^{O}C. From the JCPDS file no.10-0425 we can determine the phases present in the beads which are y-alumina (75%) and α-alumina (25%). By analysis of XRD pattern from JCPDS file it becomes clear that alumina calcined at 900^{o}C belongs to cubic crystal system of the space group ***Fd3m*** and having space group number 227.

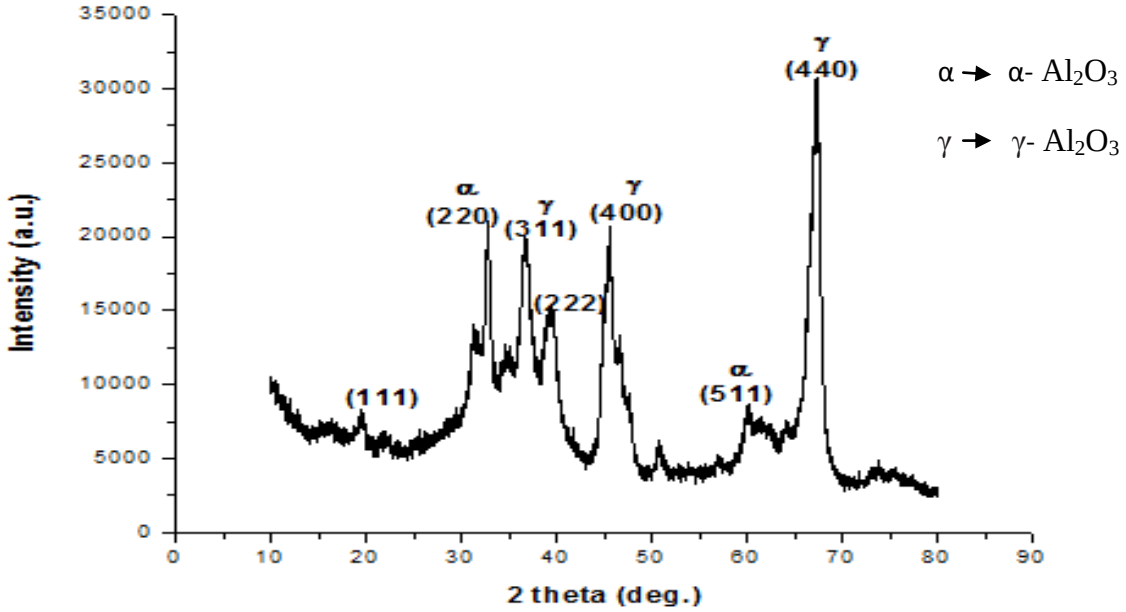

Fig. 4.3 Diffraction pattern of alumina beads (12% solid loading of boehmite) calcined at 1000^{O}C

The above figure shows the diffraction pattern of porous alumina beads calcined at 1000^{O}C. From the JCPDS file no. 46-1131 we can determine the phases present in the calcined beads which are γ-alumina and α-alumina. By analysis of XRD pattern from JCPDS file it becomes clear that alumina calcined at 1000^{o}C belongs to tetragonal crystal system of the space group ***P-4m2*** and having space group number 115.

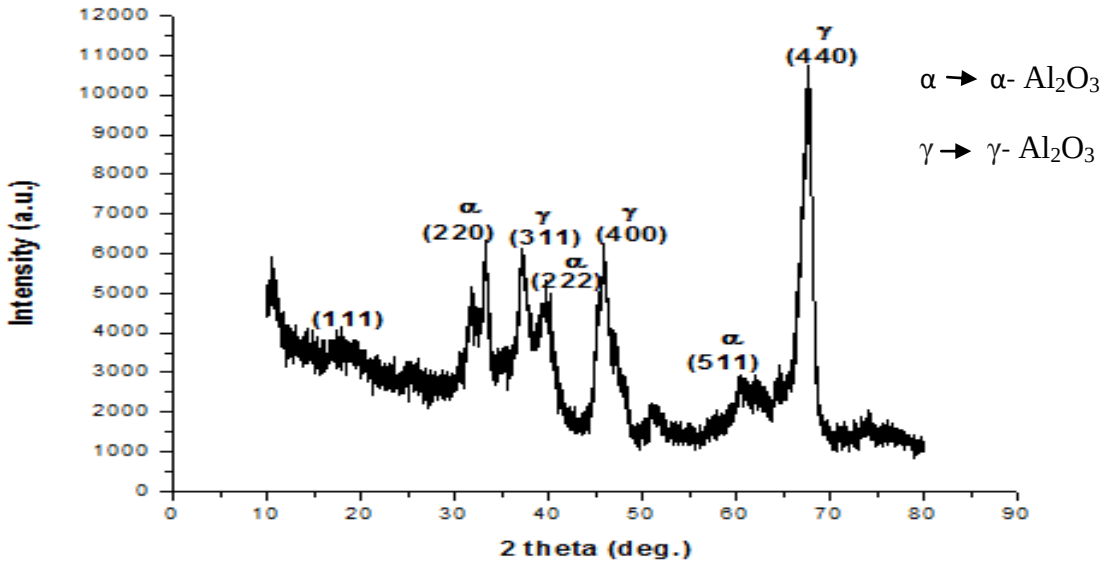

Fig. 4.4 Diffraction pattern of alumina beads (12% solid loading of boehmite) calcined at 1100^{O}C

The above figure shows the diffraction pattern of porous alumina beads calcined at 1100^{O}C. From the JCPDS file no.47-1771 we can determine the phases present in the calcined beads which are γ-alumina and α-alumina. By analysis of XRD pattern from JCPDS file it becomes clear that alumina calcined at 1100^{o}C belongs to tetragonal crystal system.

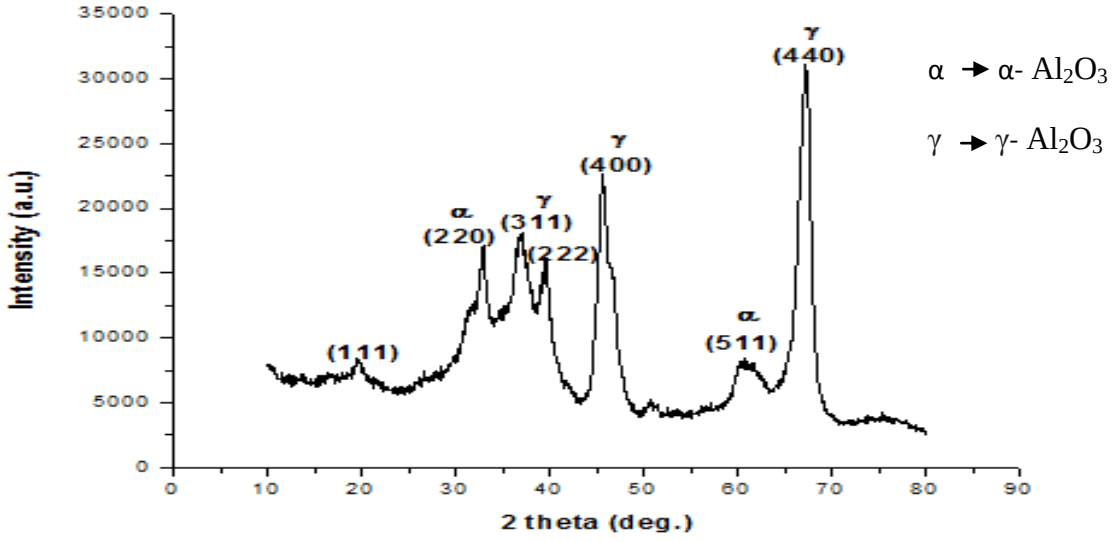

Fig. 4.5 Diffraction pattern of alumina beads (24% solid loading of boehmite) calcined at 900^{O}C

The above figure shows the diffraction pattern of porous alumina beads calcined at 900^{O}C. From the JCPDS file no. 01-1308 we can determine the phases present in the beads after calcinations which are ɣ-alumina and α-alumina. By analysis of XRD pattern from JCPDS file it becomes clear that alumina calcined at 900^{O}C belongs to cubic crystal system.

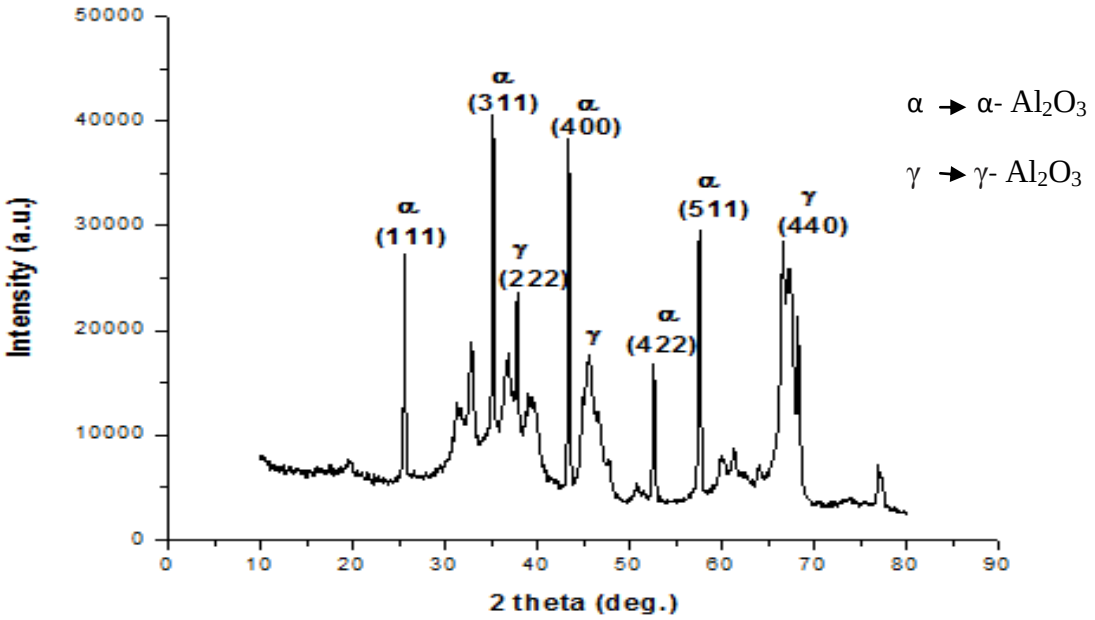

Fig. 4.6 Diffraction pattern of alumina beads (24% solid loading of boehmite) calcined at 1100^{O}C

The above figure shows the diffraction pattern of porous alumina beads calcined at 1100^{O}C. From the JCPDS file no. 42-1468 we can determine the phases present in the beads after calcinations which are ɣ-alumina and α-alumina. By analysis of XRD pattern from JCPDS file it becomes clear that alumina calcined at 900^{O}C belongs to rhombohedral crystal system. of the space group ***R-3C*** and having space group number 167.

4.3. ***Scanning Electron Microscopy (SEM)***

S112

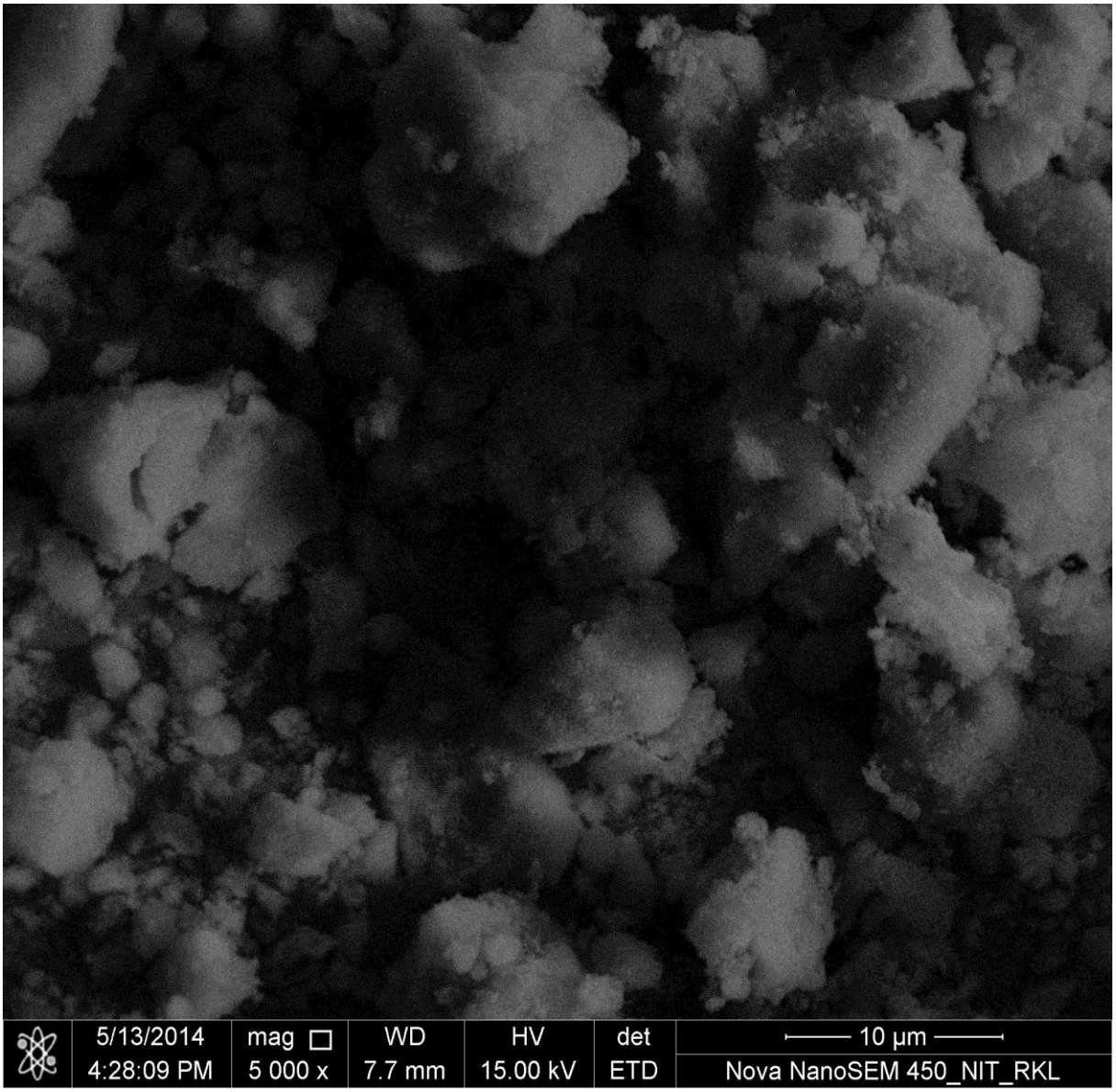

(5000X MAGNIFICATION)

Fig. 4.7 SEM Images of S112 sample (12% solid loading of boehmite) calcined at 900^{O}C for 2 hrs.

S114

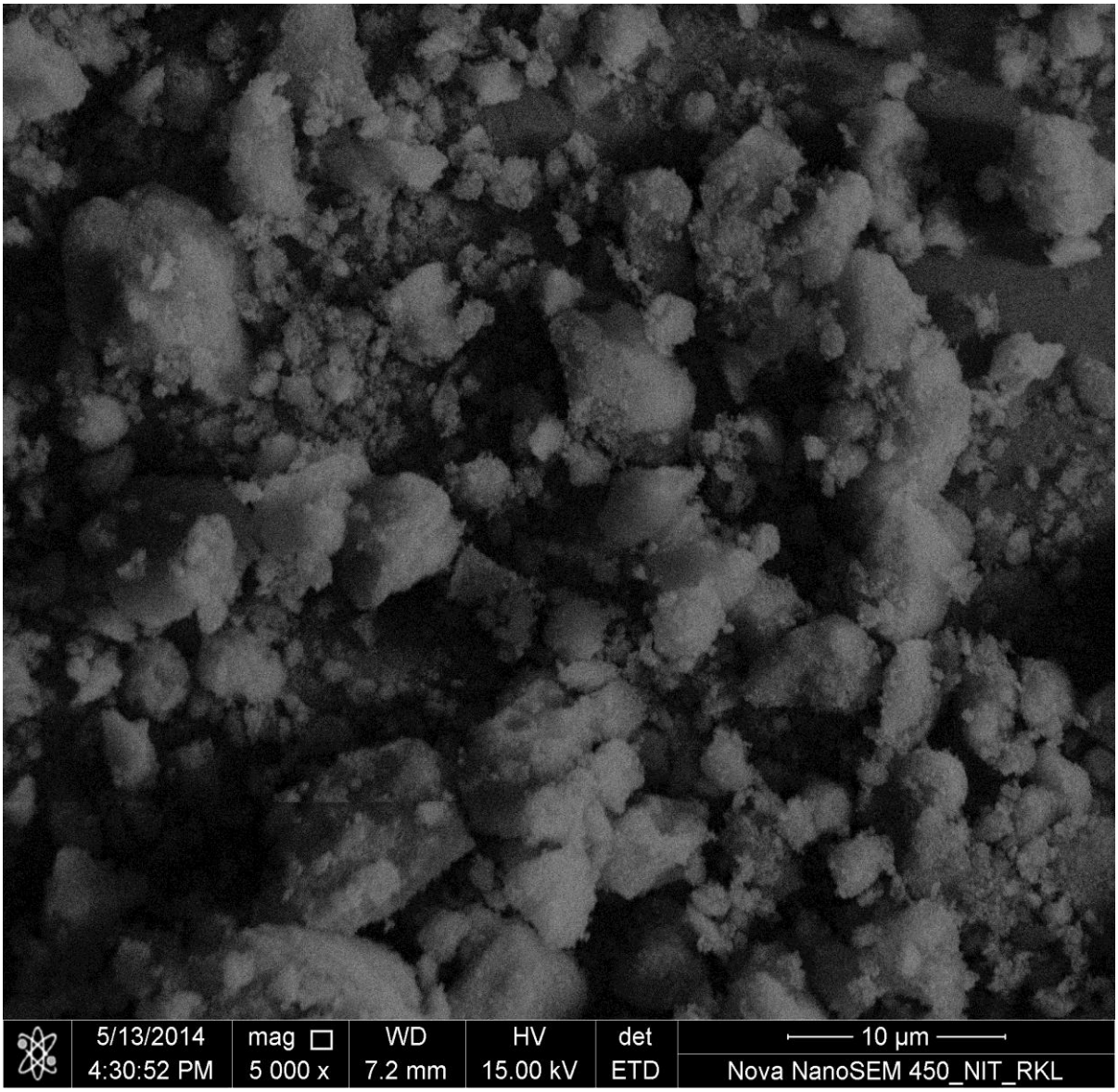

(5000X MAGNIFICATION)

Fig. 4.8 SEM Images of S114 sample (12% solid loading of boehmite) calcined at 1100^{O}C for 2 hrs.

S224

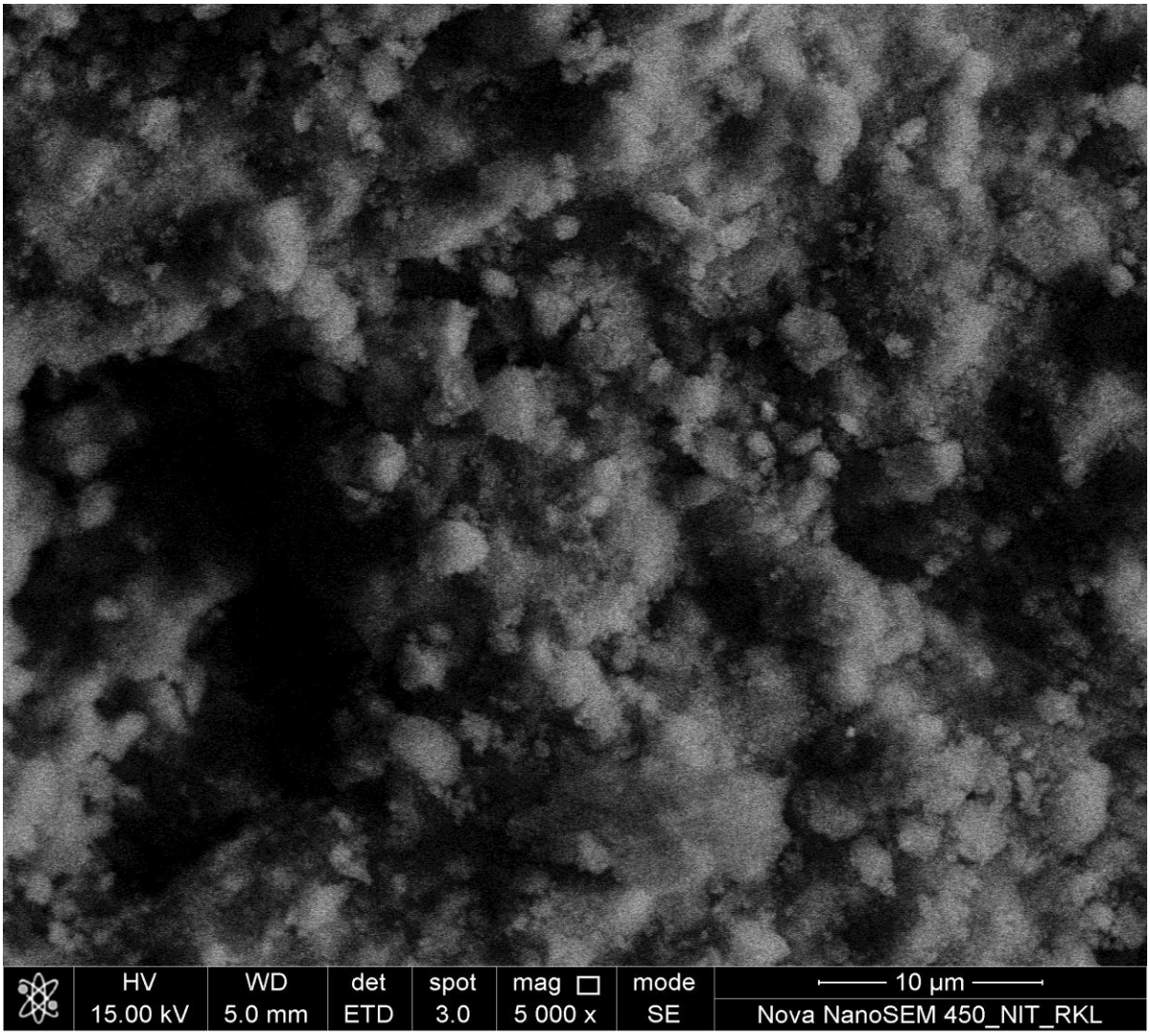

(5000X MAGNIFICATION)

Fig. 4.9 SEM Images of S224 sample (24% solid loading of boehmite) calcined at 900^{o}C for 2 hrs.

S225

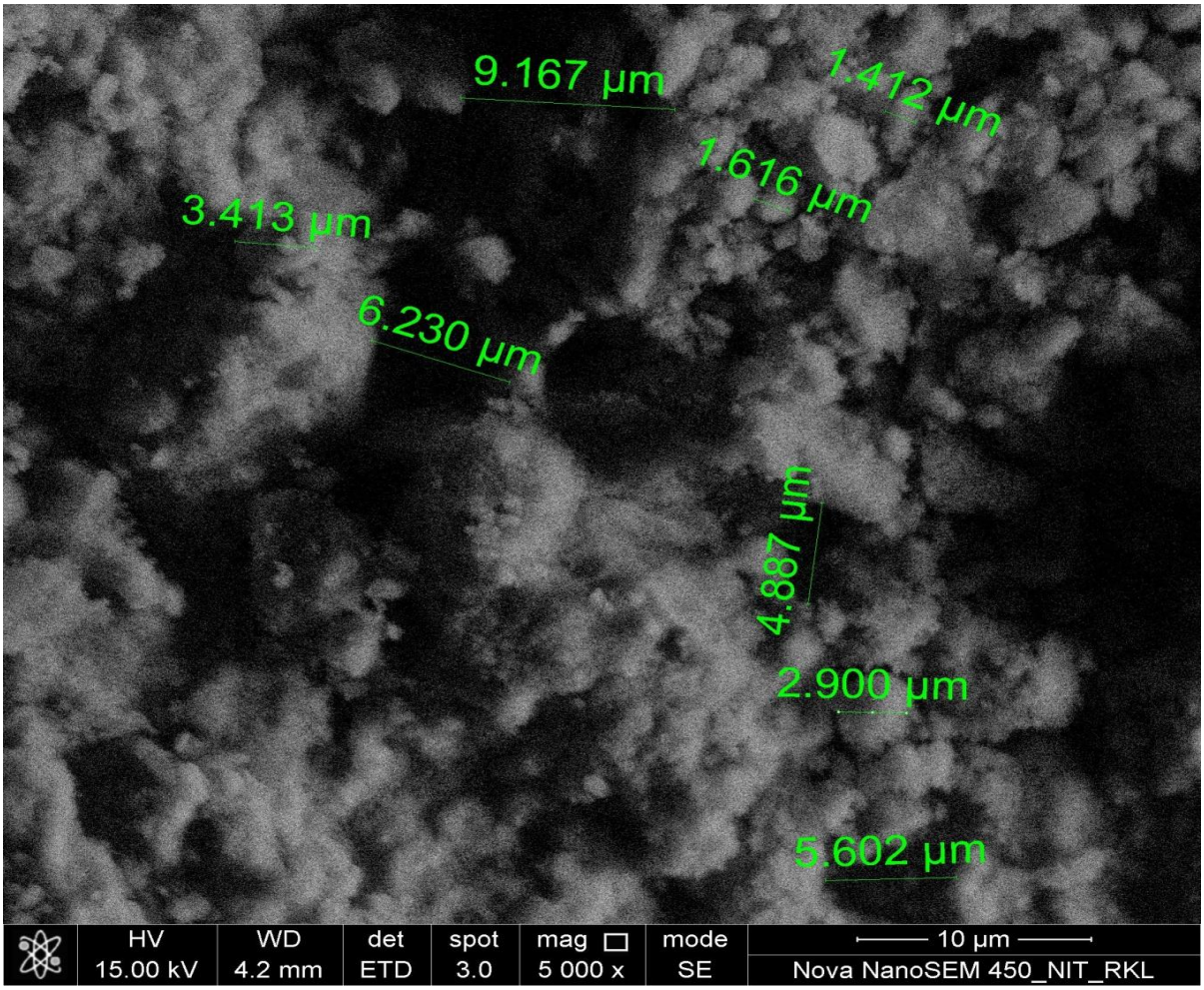

(5000 X MAGNIFICATION)

Fig. 4.10 SEM Images of of S225 sample (24% solid loading of boehmite) calcined at 1000^{O}C for 2 hrs.

S226

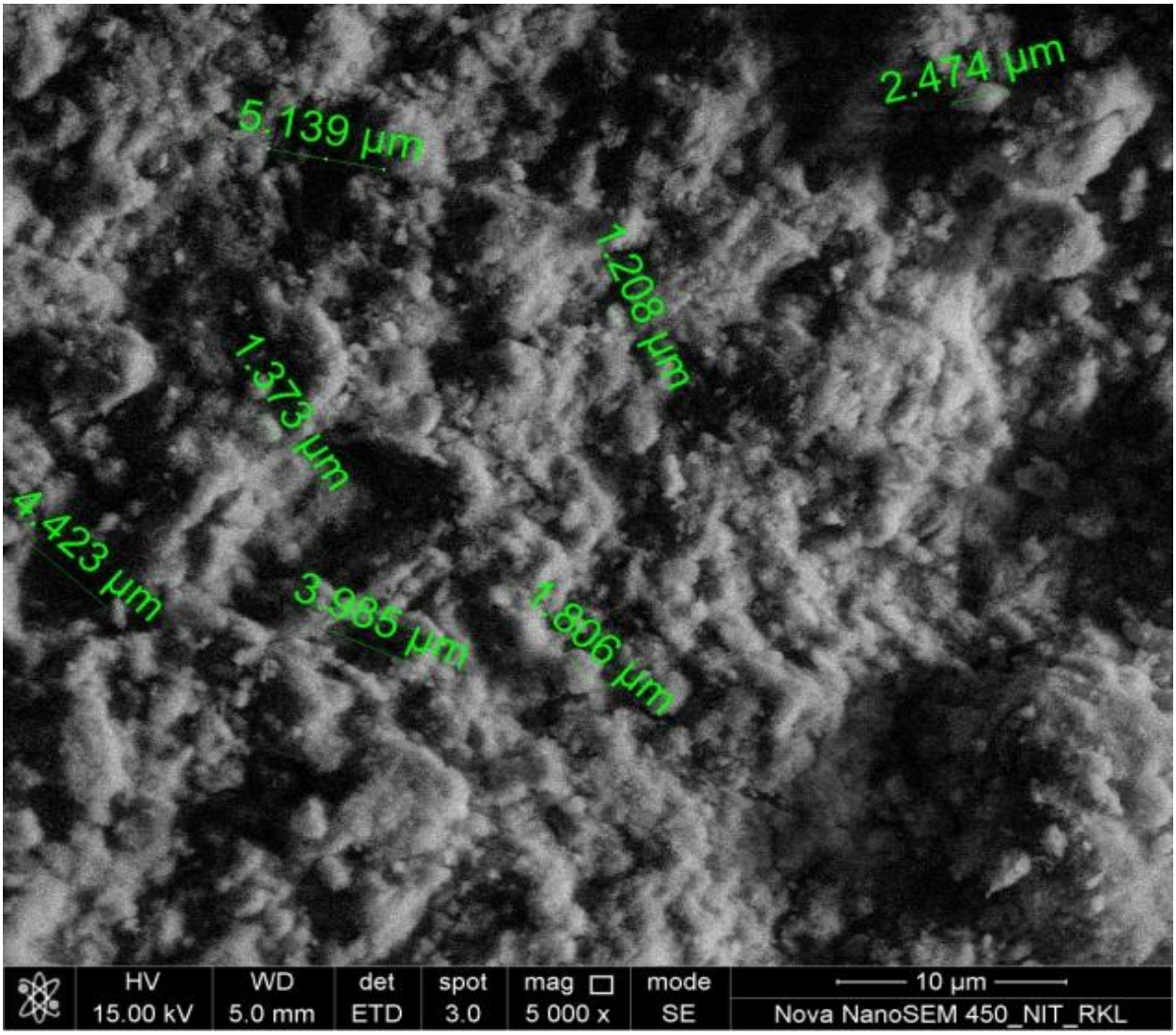

(5000X MAGNIFICATION)

Fig. 4.11 SEM Images of S226 sample (24% solid loading of boehmite) calcined at 1100^{O}C for 2 hrs.

S336

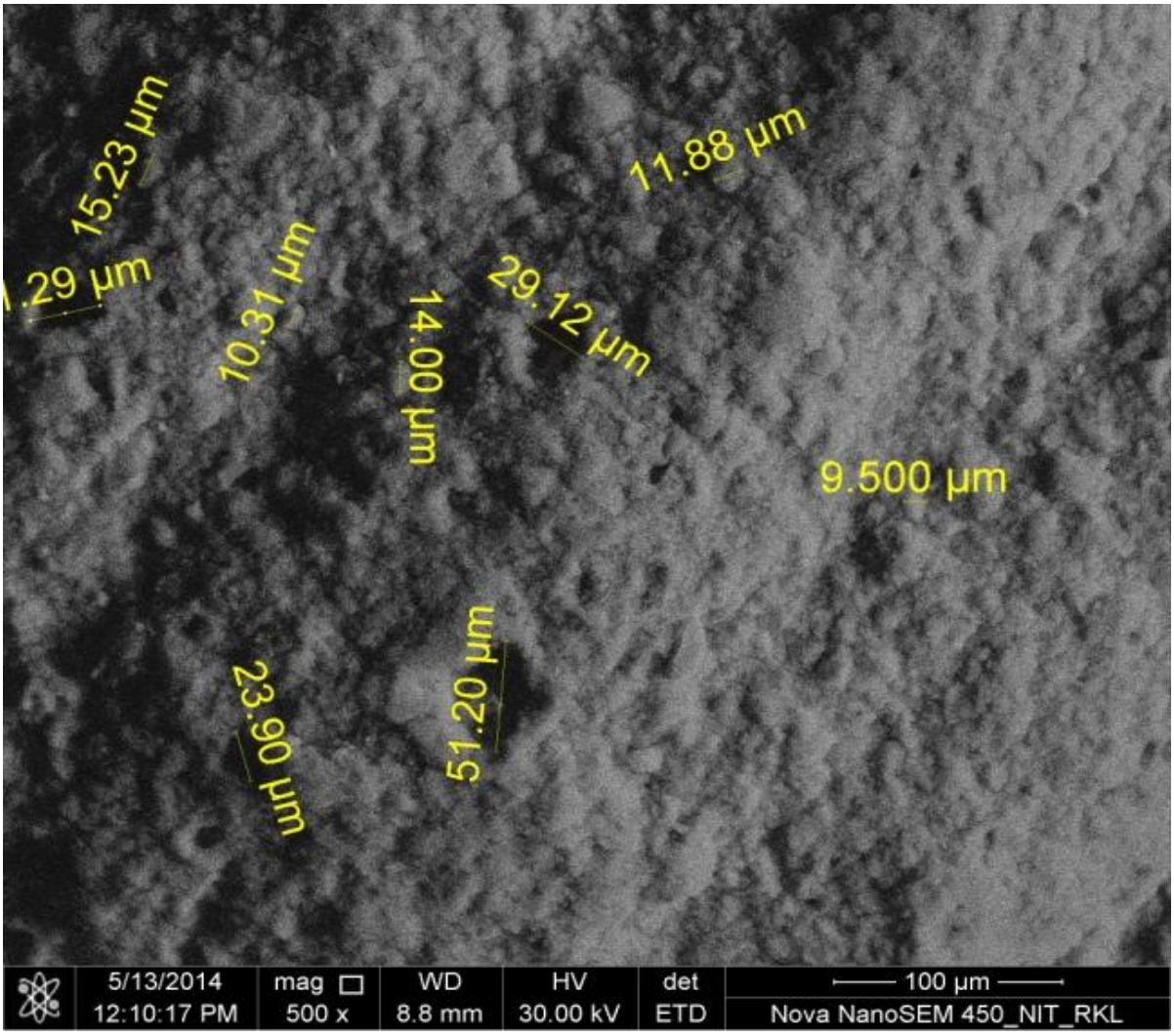

(500X MAGNIFICATION)

Fig. 4.12 SEM Images of of S336 sample (36% solid loading of boehmite) calcined at 900^{O}C for 2 hrs.

S337

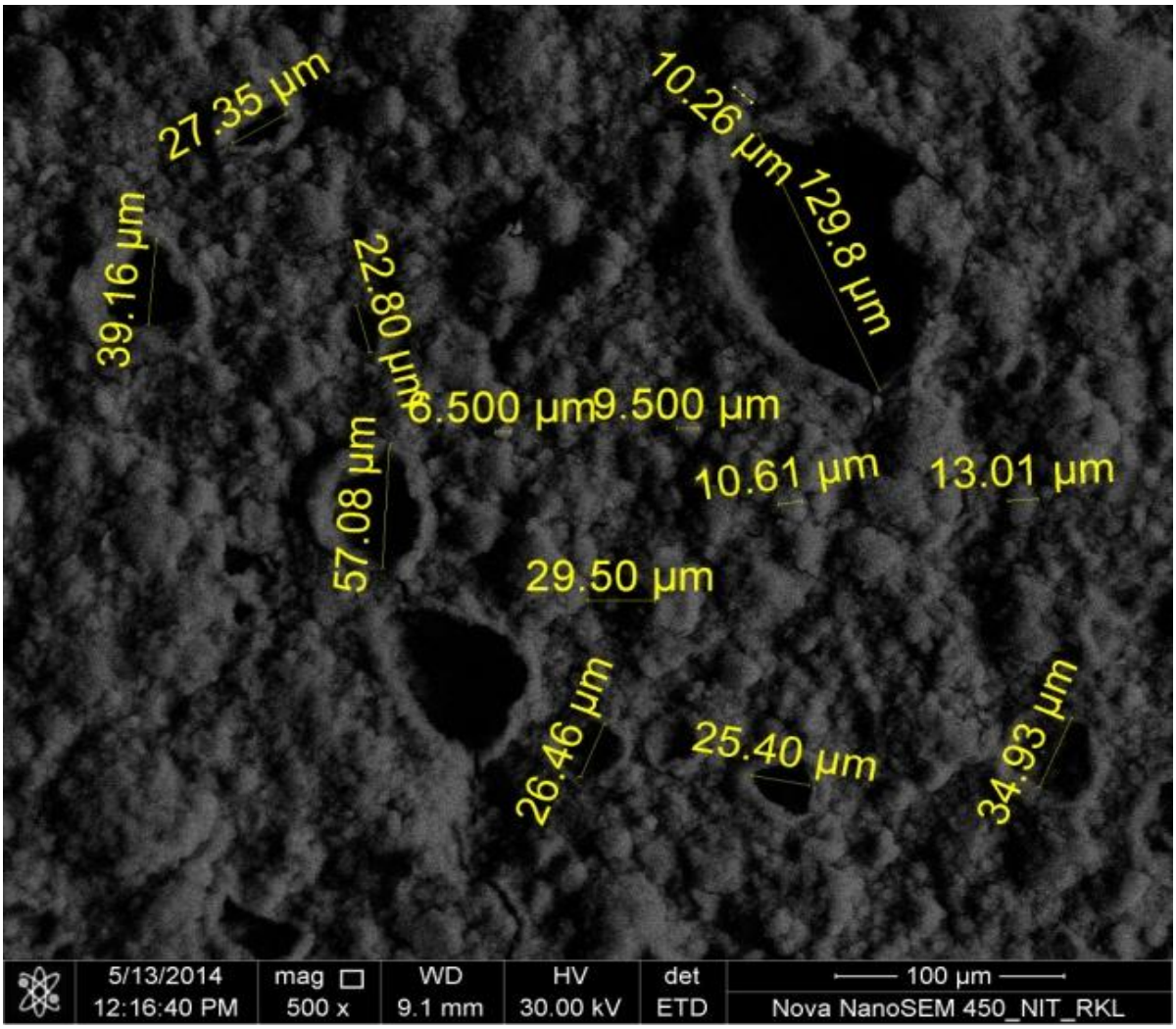

(500X MAGNIFICATION)

Fig. 4.13 SEM Images of of S337 sample (36% solid loading of boehmite) calcined at 1000^{O}C for 2 hrs.

Figures 4.7 - 4.13 show SEM images of 3 types of samples with different solid loading of boehmite (12-36%) and calcined at temperatures (900^{O}C, 1000^{O}C, 1100^{O}C) for 2 hours. The pores were clearly visible at higher magnifications. The pores were in the range of 5-130 μm. The grain size from the micrographs is found to be in the range of 3-21 μm.

Table 4.2 Summary of the pore size and grain size values of the samples analyzed from the SEM images.

Sample name	Pore size	Grain size
S224	3 - 6 μm	546 nm - 1.3 μm
S225	4.8 - 9 μm	1.4 - 4 μm
S226	4 - 6.7 μm	750 nm - 2.5 μm.
S336	24 - 51 μm	9.5 - 17 μm
S337	25 - 130 μm	3.2 - 13 μm
S338	15 - 45 μm	9.7 - 21 μm

4.4. ***BET Surface Area***

S224

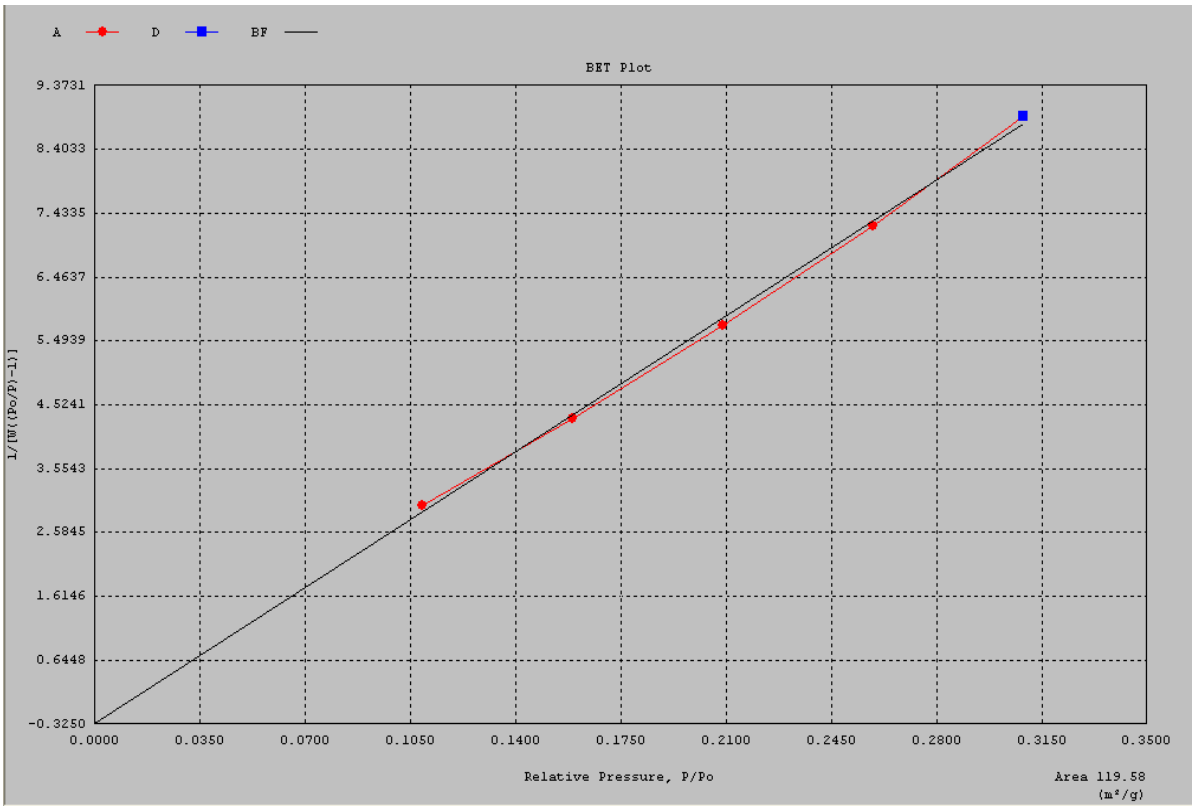

Fig. 4.15 BET Surface Area plot of S224 sample (24% solid loading of boehmite γ-alumina) calcined at 900^{O}C for 2 hrs.

From the BET Surface Area analyzer following informations were received:-

Surface Area = 119.50 m²/g

Sample Weight = 0.0186 g

Average Pore Diameter = 20.82 Å

Total pore volume = 6.223E-02 cc/g for pores smaller than 26.4 Å (Diameter), at P/Po = 0.30942

S225

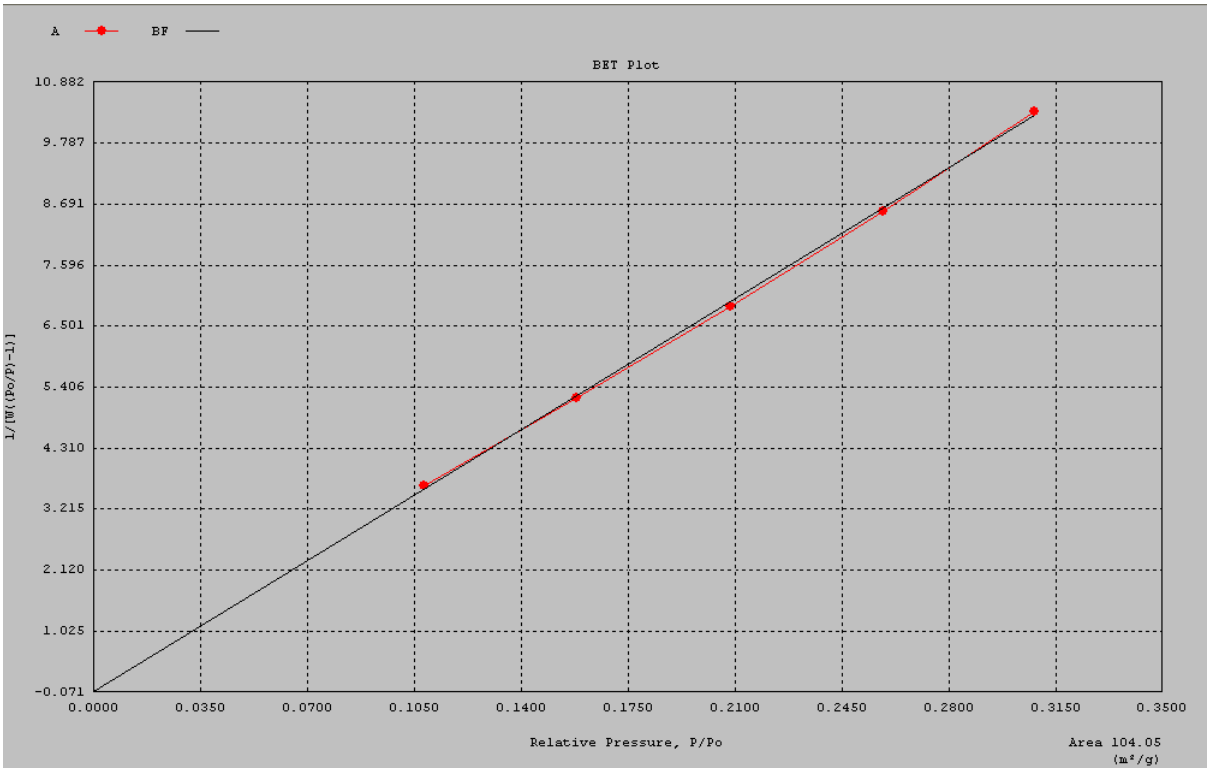

Fig. 4.16 BET Surface Area plot of S225 sample (24% solid loading of boehmite γ-alumina) calcined at 1000°C for 2 hrs.

From the BET Surface Area analyzer following informations were received:-

Surface Area = 104.05 m^2/g

Sample Weight = 0.0280 g

Average Pore Diameter = 20.49 Å

Total pore volume = 5.331E-02 cc/g for pores smaller than 26.4 Å (Diameter), at P/Po = 0.30857

S226

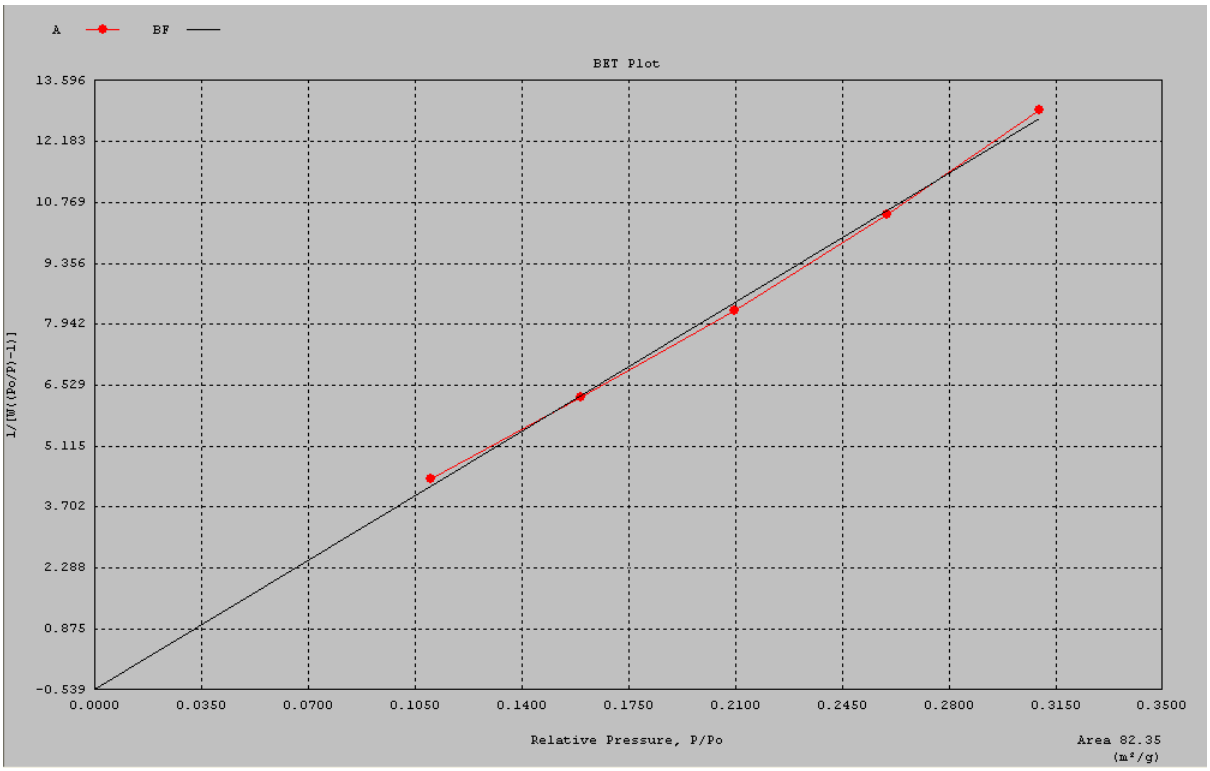

Fig. 4.17 BET Surface Area plot of S226 sample (24% solid loading of boehmite γ-alumina) calcined at 1100°C for 2 hrs.

From the BET Surface Area analyzer following informations were received:-

Surface Area = 82.35 m^2/g

Sample Weight = 0.0191 g

Average Pore Diameter = 20.88 Å

Total pore volume = 4.299E-02 cc/g for pores smaller than 26.4 Å (Diameter), at P/Po = 0.30985

S336

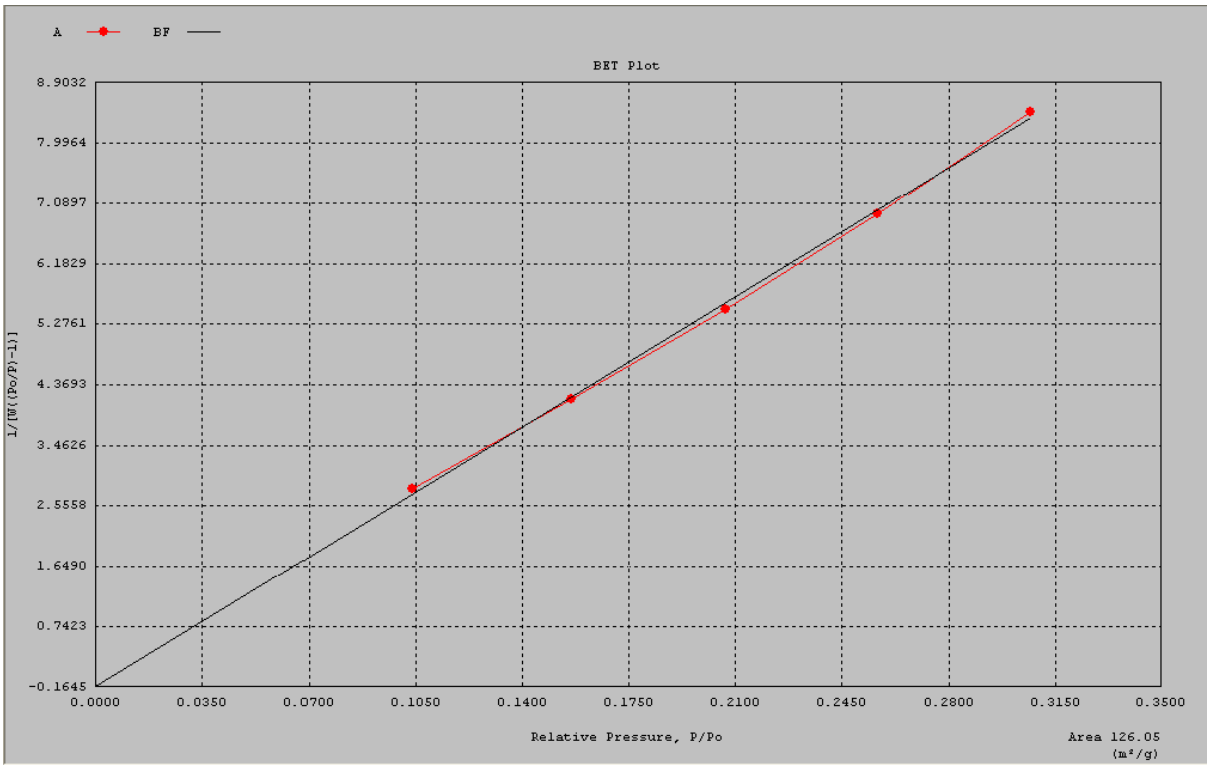

Fig. 4.18 BET Surface Area plot of S336 sample (36% solid loading of boehmite γ-alumina) calcined at 900°C for 2 hrs.

From the BET Surface Area analyzer following informations were received:-

Surface Area = 126.06 m^2/g

Sample Weight = 0.0391 g

Average Pore Diameter = 20.56 Å

Total pore volume = 6.480E-02 cc/g for pores smaller than 26.3 Å (Diameter),

at P/Po = 0.30728

S337

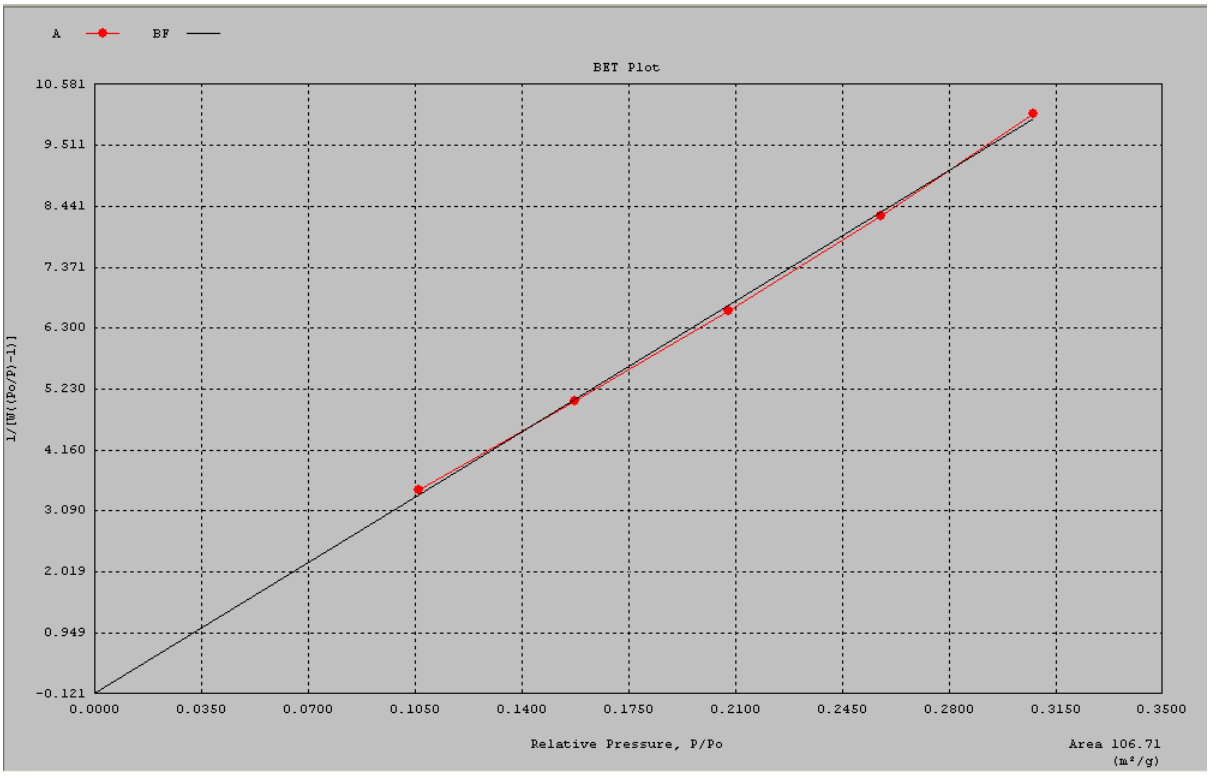

Fig. 4.19 BET Surface Area plot of S337 sample (36% solid loading of boehmite γ-alumina) calcined at 1000°C for 2 hrs.

From the BET Surface Area analyzer following informations were received:-

Surface Area = 106.71 m^2/g

Sample Weight = 0.0350 g

Average Pore Diameter = 20.45 Å

Total pore volume = 5.471E-02 cc/g for pores smaller than 26.3 Å (Diameter), at P/Po = 0.30806

S338

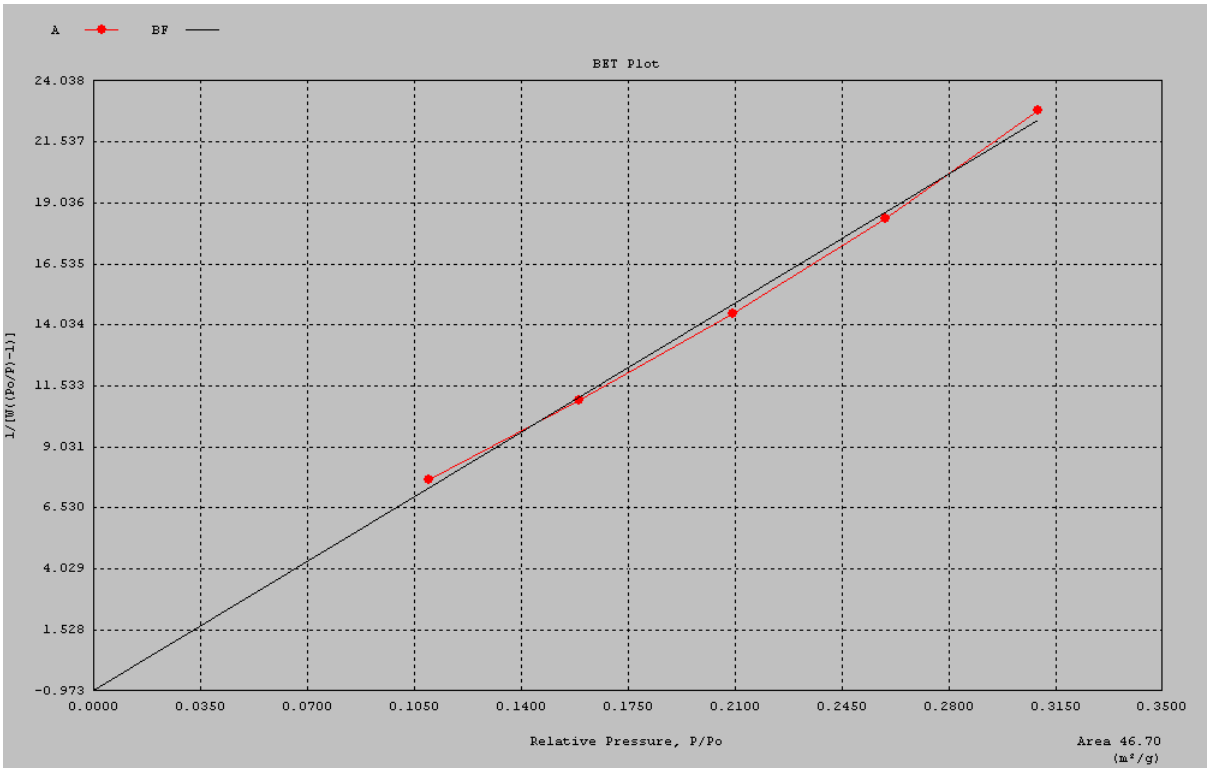

Fig. 4.20 BET Surface Area plot of S338 sample (36% solid loading of boehmite γ-alumina) calcined at 1100°C for 2 hrs.

From the BET Surface Area analyzer following informations were received:-

Surface Area = 46.70 m²/g

Sample Weight = 0.0430 g

Average Pore Diameter = 20.83 Å

Total pore volume = 2.432E-02 cc/g for pores smaller than 26.4 Å (Diameter),

at P/Po = 0.30983

From figures 4.12 - 4.18 and the above information, we get idea about surface area, average pore size and total pore volume of the beads calcined at temperatures i.e. 900°C, 1000°C, 1100°C for 2 hrs. Also from the values it can be seen that the surface area of the calcined beads decreases with higher calcination temperatures for different solid loading.

It can be inferred that the beads with 36% solid loading calcined at 900^{O}C has higher surface area when compared with others. In catalysis, high surface area is preferred.

Table 4.3 Summary of surface area, average pore diameter and pore volume of the samples analyzed by BET surface area analyzer

Sample name	P/Po	Surface Area (m^2/g)	Average Pore Diameter (Å)	Total pore volume (cc/g)
S224	0.30942	119.50	20.82	6.223E-02
S225	0.30857	104.05	20.49	5.331E-02
S226	0.30985	82.35	20.88	4.299E-02
S336	0.30728	126.06	20.56	6.480E-02
S337	0.30806	106.71	20.45	5.471E-02
S338	0.30983	46.70	20.83	2.432E-02

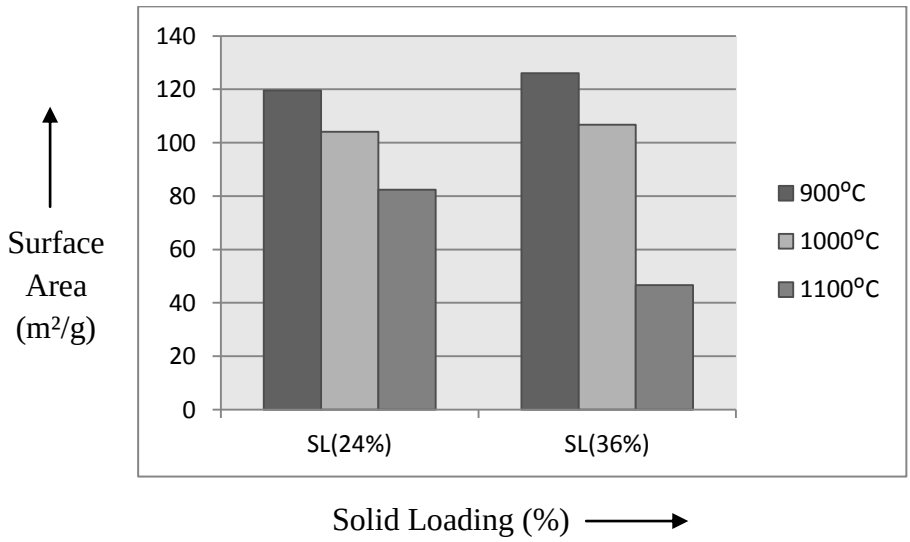

Fig. 4.21 Variation of surface area with increase in solid loading at elevated temperatures (i.e. 900°C, 1000°C, 1100°C)

4.5 ***Cold Crushing Strength (CCS) Test***

Table 4.4 Summary of average CCS values of beads with 12% solid loading of boehmite and calcined at 900^{O}C, 1000^{O}C and 1100^{O}C for 2 hrs

Sample name	Cold Crushing Strength (N)
S112	14.8
S113	17.8
S114	20.2

Table 4.5 Summary of average CCS values of beads with 24% solid loading of boehmite and calcined at 900^{O}C, 1000^{O}C and 1100^{O}C for 2 hrs

Sample name	Cold Crushing Strength (N)
S224	15.3
S225	18.51
S226	21.12

Table 4.6 Summary of average CCS values of beads with 36% solid loading of boehmite and calcined at 900^{O}C, 1000^{O}C and 1100^{O}C for 2 hrs

Sample name	Cold Crushing Strength (N)
S336	16.62
S337	19.06
S338	24.42

Table 4.4-4.6 shows hardness values of samples with different solid loading and calcined at 3 different temperatures. From the above values it becomes clear that beads with 36% solid loading exhibit higher average mechanical strength in comparison to others. Beads with 36 % solid loading and calcined at 1100°C shows highest hardness value. Also from the values it can be seen that the hardness of the calcined beads increases with higher calcination temperatures for different solid loading.

CHAPTER-5:

CONCLUSIONS

With accomplished experimentals, the conclusions could be drawn as following. The salient observations were:

1) From the diffraction pattern of samples with different solid loading it becomes clear that in calcined beads, γ-alumina as main phase as desired although trace amounts of α-alumina is present at all 3 calcined temperatures. In catalysis, γ-alumina is preferred phase to perform the job.

2) The BET surface area results gives excellent information about surface area, average pore diameter and total pore volume of the calcined samples with different solid loading. Also from solid loading vs surface area plot it can be concluded that the surface area of the calcined beads decreases with higher calcination temperatures. The decreasing trend aforementioned is common for all solid loading.

3) From the shrinkage data it becomes clear that both linear and volume shrinkage decreases with increase in solid loading of boehmite, i.e. shrinkage is high for 12% solid loading.

4) SEM images show the presence of both macro and micro pores. The pores were clearly visible at higher magnifications. The pores were in the range of 5-130 μm. The grain size from the micrographs is found to be in the range of 3-21 μm.

5) From cold crushing strength values of the calcined beads it can be inferred that mechanical strength of beads increases with increase in solid loading and calcination temperatures. While going with higher calcination temperature the strength is increased.

So to obtain the optimum mechanical strength specific areas of the beads are sacrificed to some extent. Further work and study needed to conclude the appropriate combination of strength and specific surface area.

REFERENCES

1) L.M. Sheppard, Porous ceramics: processing and applications, Ceram. Trans. 31 (1993) pp. 3–23.

2) K. Umehara, "Porous Cordierite Honeycomb for Exhaust Emission Control (in Japan), Ceram. Jpn., 33, pp. 530–33 (1998).

3) R. W. Rice," Porosity of Ceramics," pp. 539. Marcel Dekker Inc, New York, 1998

4) M. Scheffler, P. Colombo and Cellular Ceramics," Structure, Manufacturing, Properties and Applications," p. 645, Weinheim, Wiley-VCH, 2005

5) L. J. Gauckler, M.M. Waeber, C. Conti, and M. Jacobduliere," Ceramic Foam for Molten Metal Filtration," J. Metals, 37 [9] pp. 47–50 (1985)

6) J. Cao, C. R. Rambo, and H. Sieber," Preparation of Porous Alumina Ceramics by Biotemplating of Wood," J. Por. Mat. (2004), Vol. 11, Issue 3, pp 163-172

7) Elinaga, H.; Futamura, S. Comparative study on the catalytic activities of alumina-supported metal oxides for oxidation of benzene and cyclohexane with ozone. React. Kinet. Catal. Lett., 2004, 81(1), pp 121-128.

8) Bahaduri, S.; Zhou, E.; Bhaduri, S.B. Auto ignition processing of nanocrystalline α-alumina. Nanostruct. Mater., 1996, 7(5), pp. 487-496.

9) Bahlawane, N.; Watanabe, T. New sol-gel route for the preparation of pure γ-alumina at 950°C. J. Am. Ceram. Soc., 2000, 83(9), pp 2324-2326.

10) Ya. Guzman," Certain Principles of Formation of Porous Ceramic structures, Properties and Applications (a review)," J. Por. Mat. , No. 9, pp. 28-31, September 2003

11) E. J. A. E. Williams, J. R. G. Evans," Expanded Ceramic Foam," J. Mat. Sci., Vol. 31, 1996, pp. 559-563

12) O. Lyckfeldt, J. M. F. Ferreira," Processing of Porous Ceramics by 'Starch Consolidation'," J. Eur. Ceram. Soc., Vol. 18, Issue 2, 1998, pp. 131-140

13) R. Svinka, V. Svinka, I. Zake, A. Butlers,"Influence of Some Additives on the Properties of Porous Alumina Ceramics," ISSN 1392-1231, 2009

14) Kazutaka Kamitani, Takeo Hyodo, Yasuhiro Shimizu and Makoto Egashira," Fabrication of Highly Porous Alumina-Based Ceramics with Connected Spaces by Employing PMMA Microspheres as a Template," Adv. Mat. Sc. and Engg., Vol. 2009 (2009), Article ID 601850, 9 Pages

15) Andre´ R. Studart, Urs T. Gonzenbach, Elena Tervoort, and Ludwig J. Gauckler," Processing Routes to Macroporous Ceramics: A Review," J. Am. Ceram. Soc., 89 [6] pp. 1771–1789 (2006)

16) M. D. M. Innocentini, P. Sepulveda, V. R. Salvini, V. C. Pandolfelli, and J. R. Coury, ''Permeability and Structure of Cellular Ceramics: A Comparison Between Two Preparation Techniques,'' J. Am. Ceram. Soc., 81 [12], pp. 3349–3352 (1998)

17) P. Sepulveda," Gelcasting Foams for Porous Ceramics,'' Am. Ceram. Soc. Bull., 76 [10] pp. 61– 65 (1997)

18) A. J. Sherman, R. H. Tuffias, and R. B. Kaplan, ''Refractory Ceramic Foams—A Novel, New High-Temperature Structure,'' Am. Ceram. Soc. Bull., 70 [6] pp. 1025–1029 (1991).

19) C. R. Rambo and H. Sieber," Novel Synthetic Route to Biomorphic Al2O3 Ceramics,'' Adv. Mater., 17 [8] 1088 (2005)

20) P. Greil: Biomorphous Ceramics from Lignocellulosics,'' J. Eur. Ceram. Soc., 21 [2] pp. 105–118 (2001)

21) J. Cao, C. R. Rambo, and H. Sieber," Preparation of Porous Alumina Ceramics by Biotemplating of Wood," J. Por. Mat. (2004), Vol. 11, Issue 3, pp. 163-172

22) P. Greil, ‘‘Biomorphous Ceramics from Lignocellulosics,’’ J. Eur. Ceram. Soc., 21 [2] pp. 105–118 (2001).

23) C. Zollfrank, N. Travitzky, H. Sieber, T. Selchert, and P. Greil, ‘‘Biomorphous SiSiC/Al–Si Ceramic Composites Manufactured by Squeeze Casting: Microstructure and Mechanical Properties,’’ Adv. Eng. Mater., 7 [8] pp. 743–746 (2005).

24) C. Ritzoulis, N. Scoutaris, K. Papademetriou, S. Stavroulias, and C. Panayiotou, ‘‘Milk Protein-Based Emulsion Gels for Bone Tissue Engineering,’’ Food Hydrocolloids, 19 [3] pp. 575–581 (2005).

25) A. Imhof and D. J. Pine, ‘‘Ordered Macroporous Materials by Emulsion Templating,’’ Nature, 389 [6654] pp. 948–951 (1997).

26) Dibyendu Chakravarty, Hayagreev Ramesh, Tata N. Rao,” High Strength Porous Alumina by Spark Plasma Sintering” J. Eur. Ceram. Soc., Vol. 29, 2009, pp. 1361–1369

27) Andre´ R. Studart, Urs T. Gonzenbach, Elena Tervoort, and Ludwig J. Gauckler,” Processing Routes to Macroporous Ceramics: A Review,” J. Am. Ceram. Soc., 89 [6] pp. 1771–1789 (2006)

28) P. Colombo and J. R. Hellmann,” Ceramic Foams from Preceramic Polymers,’’ Mater. Res. Innovations, 6 [5–6] pp. 260–272 (2002)

29) L. L. Wood, P. Messina, and K. Frisch. ‘‘Method of Preparing Porous Ceramic Structures by Firing a Polyurethane Foam that is impregnated with Organic Materia.’’ U.S. Patent, 1974.

30) Toshihiro Isobe, Yoshikazu Kameshima, Akira Nakajima, Kiyoshi Okada Yuji Hotta,” Gas Permeability and Mechanical Properties of Porous Alumina Ceramics with Uni-Directionally Aligned Pores,” J. Eur. Ceram. Soc., Vol. 27, Issue 1, 2007, pp. 53-59

31) R.M. Heck, R.J. Ferrauto and S.T. Gulati, Catalytic Air Pollution Control – Commercial Technologies (Wiley Interscience, 2002).

32) Weijiang Xue, Yang Sun, Yong Huang, Zhipeng Xie, Jialin Sun," Preparation and Properties of Porous Alumina with Highly Ordered and Unidirectional Oriented Pores by a Self- Organization Process," J. Amer. Ceram. Soc., Vol. 94, Issue 7, pp. 1978–1981, July 2011